Emission Control Science and Technology (2026) 12:26
https://doi.org/10.1007/s40825-026-00307-9

RESEARCH

An Approximate Algebraic Model for Conversion and Light-off Curves by First-order Reactions in Monolith Converters Operated in the Graetz Regime

Martin Wörner[1]

Received: 11 February 2026 / Revised: 23 July 2026 / Accepted: 30 July 2026
© The Author(s) 2026

Abstract
The interaction of mass transfer with irreversible first order heterogeneous-homogeneous chemical reactions in an isothermal circular channel with laminar Poiseuille velocity profile is investigated theoretically. Starting from a novel approximate solution for the reactant mass balance valid in the Graetz regime with fully developed concentration field, a one-term exponential model for conversion is derived which depends on three dimensionless groups: the normalized transversal diffusion time scale (α) and the Damköhler numbers of the heterogeneous ($Da_\mathrm{w} > 0$) and homogeneous ($Da_\mathrm{b} \geq 0$) reactions. The model requires the determination of the root of a polynomial of the Damköhler numbers, which entails only minimal numerical effort. The accuracy of the model is tested for the case of a heterogeneous reaction ($Da_\mathrm{b} = 0$), showing good agreement with numerical solutions and formal analytical limits provided $\alpha \leq 1$. The proposed single channel conversion model is used to determine observed and intrinsic rate constants, as well as kinetic parameters (pre-exponential factor and activation energy), based on literature data regarding NO conversion via selective catalytic reduction in monolith reactors. In combination with temperature dependent rate constant and diffusion coefficient, the model allows studying effects of parameter variations on the light-off curve in monolith reactors within seconds. The proposed model may therefore be a useful tool for engineering design and optimization of monolith converters.

Keywords Catalytic converter · Convective diffusion with reaction · First-order reaction · Honeycomb monolith · Laminar tubular reactor · Selective catalytic reduction

1 Introduction

Catalytically coated honeycomb monolithic (that is, one-piece) supports enable heterogeneous chemical reactions [1] for many technical processes, including automotive [2], marine [3] and stationary exhaust control [4], catalytic combustion of natural gas [5], partial oxidation of methane [6] and more [7]. Channels of ceramic monoliths are often square in cross-section and have a side length of 0.5–4 mm. On the walls, the catalytically active material is deposited in a typically 10–150 µm thick porous washcoat, being thickest in the channel corners [8]. In the monolith channels, the following phenomena occur: (1) heterogeneous reactions at the catalyst wall and homogeneous (bulk) reactions in the gas phase; (2) heat, mass, and momentum transfer by convection and diffusion in the gas phase and at the gas-solid interface; (3) diffusive mass transfer in catalyst pores; (4) heat transfer by conduction and radiation in the solid [9]. The mass transfer can thus be divided into two parts: the external (or inter phase) mass transfer from the gas bulk to the channel walls, and the internal (or intra phase) mass transfer inside the porous washcoat. Because the internal part of the washcoat contains much more area than the external part, most of the reaction takes place within the pores of the washcoat. Depending on the heat of reaction, strong interactions between chemical reactions and heat/mass transfer may occur. An appropriate way to capture these interactions is to use computational fluid dynamics (CFD).

✉ Martin Wörner
martin.woerner@kit.edu

[1] Institute of Catalysis Research and Technology, Karlsruhe Institute of Technology (KIT), Engesserstr. 20, 76131 Karlsruhe, Germany

Published online: 24 August 2026

Modeling of monolith reactors for automobile emission control and other applications is a multiscale problem [10, 11]. An overview on modeling of monolith converters with references up to 1996 is given in [12] while the current status is reviewed in [13]. For an overview on advanced multichannel modeling of catalytic converters the reader is referred to [14] and references therein. Instead of modeling the entire monolith, often the single channel model (SCM) is used for simplicity. The basic assumption of the SCM is that all channels are identical and subject to the same inlet conditions. While this assumption is not valid in general, e.g., due to non-uniform flow [15] or temperature [16] distributions, several publications have shown that there are conditions where a single cylindrical channel can be representative of a monolith consisting of a multitude of rectangular channels [17, 18].

2D or 3D distributed parameter models numerically solve a set of coupled particle differential equations to determine axial and transversal variations in concentration and temperature in the channel and to appropriately account for external heat and mass transfer [19–22]. Lumped parameter 1D models consider instead axial variations of mean values [23, 24]. They require appropriate models for the external heat/mass transfer between the bulk gas stream and the wall at any axial position, i.e., local heat/mass transfer coefficients obtained from correlations for the Nusselt or Sherwood numbers. In this context it is problematic that the Nusselt and Sherwood numbers for the case in which chemical reaction occurs at the wall are not the same as those observed in either the constant wall temperature/concentration or the constant wall flux cases [25, 26]. The specific choice of the Sherwood number correlation can have a large effect on the results [8, 27, 28].

The internal mass transfer in the complex pore system depends on the porosity of the washcoat, and the geometry and shape of the pores. In classical rector modelling, diffusion and reaction occurring within the porous washcoat are not resolved. Instead, the catalyst is modeled as a continuous porous medium with an effective diffusivity. Actual reaction rates depend on the value of the (internal) effectiveness factor (η), which in turn depends on the Thiele modulus. The internal effectiveness factor relates the average, or observed, reaction rate over the entire catalyst volume to that obtained by evaluating the reaction rate at the temperature and concentration prevailing at the washcoat surface [13]; lumping the effect of washcoat diffusion into the (known) effectiveness factor allows for a simple description of diffusion limitations in the catalytic pores. Some models assume the catalytic layer to be very thin so that the effectiveness factor is equal to one [29]. Mladenov et al. [18] presented a thorough numerical investigation of monoliths with non-uniform washcoat, along with various channel geometries, using models of varying complexity − from simple 1D models with effectiveness factors to complete 2D and 3D CFD models coupled with multidimensional reaction-diffusion models.

Very advanced multidimensional models include terms for catalytic reaction, heat and mass transfer between the channel wall and the gas, axial conduction in the solid wall, and heat exchange by radiative transfer and solve mass balances for gaseous flow and in the porous washcoat. The computational cost of such simulations, however, renders them unsuitable for design or optimization studies where a large number of simulation runs are necessary. Advanced reduced-order models use axial balances plus effective internal/external mass-transfer coefficients to replace the full 3D pore-scale problem; this gives a speed up of order of magnitudes and allows for real time transient simulations of monolith reactor with multiple washcoat layers [30–32].

In some cases, analytical models can offer an alternative to numerical models; an example in emission control are particulate filters [33–35]. Analytical models have the advantage over numerical models of faster solution and they make the identification of general trends easier. Also, an analytical expression is more convenient for engineering calculation and is also the obvious starting point for a better understanding. Competing laminar flow with reaction and radial heat and mass transfer by diffusion in a single channel represents a generalized Graetz-Nusselt problem and is amenable to analytical solution. Many generalized Graetz problems are reducible to self-adjoint Sturm–Liouville problems, including heterogeneous reactions on the tube walls and homogeneous reactions in the gas phase [36]. The local reactant distribution can then be computed by truncating an infinite sum of eigenmodes which are often Laguerre functions [37, 38]. However, for each value of the rate constant a potentially large number of eigenvalues need to be calculated numerically.

The objective of the present study is to derive theoretically a simple yet sufficiently accurate one-term exponential model for the conversion of chemically reacting laminar flow which is suitable to support the engineering design of monolith reactors. In contrast to similar models from literature, the present model does not require the specification of an external mass transfer coefficient [39] or Sherwood number [40, 41]. For simplicity, the present treatment is restricted to a single cylindrical channel under steady-state isothermal conditions. The flow field is assumed to be unaffected by mass transport and the laminar (Poiseuille) flow profile is prescribed. The chemical reactions are assumed to be first-order in the local reactant concentration. Irreversible single homogeneous and catalytic wall reactions are considered. Potential diffusion limitations in the porous washcoat are taken into account by incorporating the effectiveness factor into the observable rate constant. These assumptions allow for a simplified mathematical treatment by considering the local mass balance equation of the

reactant only. For the latter, a novel approximate solution is determined which properly accounts for external mass transfer. The approximate solution is used to derive a one-term exponential model for conversion that depends on three distinct dimensionless groups, the normalized transversal diffusion time scale and two Damköhler numbers. The model enables a comparison with experimental light-off curves with minimal numerical effort.

The paper is organized as follows. Section 2 presents the mathematical problem, along with its underlying simplifying assumptions. The novel approximate solution for the overall conversion is presented in Sect. 3. In Sect. 4, the one-term model for overall conversion is tested by comparison with experimental light-off curves obtained for the selective catalytic reduction (SCR) of nitrogen monoxide.

2 Problem Formulation

This section introduces the model assumptions and presents the simplified partial differential equation for the reactant mass balance which forms the basis for modelling.

2.1 Model Assumptions

2.1.1 Single Channel Model

The conditions in the monolith converter are assumed to be identical in all honeycomb channels. This implies a uniform catalyst distribution, an equally distributed inlet flow over the entire cross section of the honeycomb, and an ideal homogeneous premixing of the exhaust gas and reductant mixture. According to these idealizing assumptions, the simulation of the physicochemical processes occurring in the monolith converter is reduced to the analysis of one representative single channel.

For the mathematical treatment, we approximate the channel by a circular cylinder (radius a, diameter $d = 2a$, length L), similar to previous studies [42]. We employ a cylindrical coordinate system where the distance from the axis of the tube (r) is in the range $0 \leq r \leq a$ and the axial coordinate z is in the range $0 \leq z \leq L$. In reality, the cross-section of monolith channels is often square or triangular with rounded corners. To apply the present model − developed for circular channels − to other channel geometries, we draw upon the theory of shape normalization for catalytic monoliths [43, 44].

2.1.2 Uniform Temperature

In this paper, temperature gradients within a single monolith channel are assumed small so that the problem can be considered as isothermal. This assumption can be reasonable for emission control in automotive applications and stationary power plants where heat effects as a result of the reaction are often of minor importance since reactants concentrations are typically in the ppm-range and the amount of heat generated by the reaction in a dilute system with a large fraction of inert gas is low. It is invalid for oxidation reactions [45] and catalytic combustion [5], where the axial temperature profile in the monolith channels typically rises sharply near the inlet due to reaction ignition, reaches a maximum shortly after light-off, then gradually declines toward the outlet due to heat losses and reaction completion (and hence no further heat generation). A more general and systematic analysis of the effect of spatial temperature profiles on reactions in tubular reactors is given in [46].

With the isothermal channel assumption, which is also used in related analytical [43, 44] and numerical studies [47–49], the corresponding spatially uniform temperature (T) in the channel is an input parameter of the model. Rate constants and physical properties of the gas and reactant are then constants at a given temperature and pressure. Results of the isothermal channel model obtained at different temperatures are presented in Sect. 4.

2.1.3 Fully Developed Poiseuille Velocity Profile

To determine the actual local gas velocity within the channel, the rigorous solution of momentum balance and continuity equations is required. This is avoided here by introducing further assumptions. Typical monolithic reactors in automobile exhaust applications work in the laminar flow regime and have a negligible pressure drop. Compressibility effects are neglected, the density and further physical properties of the isothermal gas mixture are assumed constant and its flow is described as an incompressible viscous Newtonian fluid (kinematic viscosity ν). The channel Reynolds number $Re = 2aU/\nu$ is typically in the range 50–100 [50]. The hydrodynamic entrance region is then a small fraction of the overall channel length, which also holds for higher Reynolds number of $Re = 408$ [20]. Similar to [51, 52], we therefore assume right from the channel inlet a fully developed unidirectional steady-state and axi-symmetric laminar flow so that the velocity profile is parabolic (Poiseuille flow) with mean velocity U and maximum velocity $2U$.

2.2 Reactant Mass Balance

Due to the assumptions of isothermal operation in combination with a pre-scribed velocity profile, neither a thermal energy balance nor a momentum balance is required. The present model can therefore be developed using only the mass balance, similar to the model in [47]. If a chemical

species is undergoing a first-order reaction, only the mass balance of this single component needs to be considered, since the reaction term is independent of the concentration of other components. Here we assume that the concentration of the reactive species is rotationally symmetrical around the z axis and denote its molar concentration at time t by $c(r, z, t)$.

With the mentioned assumptions, the general unsteady mole balance equation for a single dilute species undergoing a first-order irreversible homogeneous chemical reaction may be written in terms of molar concentration as

$$\begin{aligned} &\frac{\partial c}{\partial t} + 2U\left(1 - \frac{r^2}{a^2}\right)\frac{\partial c}{\partial z} \\ &= D\left[\frac{1}{r}\frac{\partial}{\partial r}\left(r\frac{\partial c}{\partial r}\right) + \frac{\partial^2 c}{\partial z^2}\right] - k_{\mathrm{b}} c \end{aligned} \tag{1}$$

with boundary condition $\partial c/\partial r = 0$ at the tube axis and the wall. From the rate constant of the homogeneous (bulk) reaction, k_{b}, the time scale $\tau_{\mathrm{r,b}} = 1/k_{\mathrm{b}}$ may be defined. In Eq. (1), D denotes the molecular diffusion coefficient of the reactive species in the carrier gas. We assume that the diffusion coefficient depends on temperature but not on pressure or concentration. Due to the parabolic velocity profile, there is a variation in reaction time (residence time) which causes the extent of the homogeneous reaction to vary in the radial direction. This results in a radial concentration gradient which in turn induces diffusion. While the homogeneous reaction is considered by a sink term in Eq. (1), a heterogenous reaction may be incorporated by the surface condition at the catalytically wall where the diffusional flux is equal to the wall reaction [53].

Except for extremely slow flows and at extremely short length scales, molecular diffusion in axial direction is negligible in comparison to advection. For Peclet numbers $Pe = 2aU/D$ larger than 200, the longitudinal diffusion term in Eq. (1) becomes insignificant [54]. By neglecting axial diffusion, the mole balance equation changes from elliptic to parabolic type. An analytical solution of the respective steady state problem for a homogeneous first-order reaction was first presented by Lauwerier [55]. He obtained steady solutions for the local concentration field in a tube with inlet condition $c\,(r, z = 0) = c_0$ via an orthogonal eigenfunction series expansion of the form

$$c(r, z) = \sum_{i=1}^{\infty} A_i \cdot \varphi_i(r) \cdot \psi_i(z) \tag{2}$$

Here, $\psi_i(z)$ is of exponential type while $\varphi_i(r)$ are orthogonal eigenfunctions. The associated eigenvalues are determined from the radial boundary condition at the wall. In the absence of a heterogenous reaction, the boundary condition at the wall is homogeneous. In this case the radial ODE comprises a proper Sturm-Liouville system for which there exists an infinite set of real, non-negative eigenvalues and a corresponding set of real eigenfunctions. In order to fulfill the axial boundary condition at the inlet, the coefficients A_i of the series expansion (2) are determined by means of orthogonal properties of the eigenfunctions [55]. Wissler & Schlechter [56] obtained the first few eigenvalues, expansion coefficients and other important constants in the Lauwerier solution using numerical procedures. Subramanian et al. [57] found it necessary to use up to 45 terms in the series, for the range of conversion investigated.

For any changes in the system such as the velocity profile of non-Newtonian fluids [58, 59] and consideration of homogeneous and/or heterogeneous chemical reactions, one has to develop a new set of eigenvalues, eigenfunctions, and their associated expansion coefficients according to these changes. Therefore, there are extensive tabulated and/or graphical eigenfunctions, eigenvalues, and their associated constants [54, Tab. I]. In addition, the eigenvalues and eigenfunctions can usually not be determined analytically but require a numerical procedure [54, 60–62]. In consequence, the solution becomes numerical and for every parameter of interest the whole scheme has to be repeated. Lawal [59] applied the finite integral transform technique to derive analytical solutions for the convective diffusion of power-law fluids in parallel plate and tubular reactors with single homogeneous and catalytic wall reactions. The number of terms retained in the series expansion solution was varied from 20 to 80. For such large numbers, analytical solutions offer little or no advantage over numerical solutions. In the next section, a procedure is presented which is free from these difficulties and gives an approximate analytical solution for the overall conversion which is of fairly good accuracy.

2.2.1 Normalization

We normalize the radial and axial coordinates differently and define $R = r/a$ and $Z = z/L$ so that $0 \le R \le 1$ and $0 \le Z \le 1$, respectively. We further define $C = c/c_0$ where c_0 represents the constant inlet concentration at $Z = 0$ so that $0 \le C \le 1$. We normalize time by the channel space time $\tau_{\mathrm{s}} = L/U$ and introduce the reduced time $\theta = t/\tau_{\mathrm{s}} = tU/L$. Then Eq. (1) takes the non-dimensional form

$$\begin{aligned} &\frac{\partial C}{\partial \theta} + 2(1 - R^2)\frac{\partial C}{\partial Z} \\ &= \frac{4\lambda}{Pe}\left[\frac{1}{R}\frac{\partial}{\partial R}\left(R\frac{\partial C}{\partial R}\right) + \frac{1}{4\lambda^2}\frac{\partial^2 C}{\partial Z^2}\right] - \frac{16\lambda}{Pe} Da_{\mathrm{b}} C \end{aligned} \tag{3}$$

where $\lambda = L/d$ is the length-to-diameter ratio of the channel. The parameter $Da_\mathrm{b} = \tau_\mathrm{d}/4\tau_\mathrm{b} = a^2 k_\mathrm{b}/4D$ is a dimensionless reaction constant (a second Damköhler number). The factor 4 in the denominator of Da_b follows the definition of Lauwerier [55, Eq. 2.5] and serves to simplify subsequent mathematical expressions. The dimensionless group $Gz = Pe/\lambda = d^2U/LD$ represents the Graetz number for mass transfer. Here, we define $\alpha = Gz/4 = a^2U/LD$. The present parameter α is identical to the transverse Peclet number P in [26, 63, 64] and the modified Peclet number Pe' in [65]. However, the term transverse Peclet number is not used consistently in the literature, as in other related references it denotes the group aU/D [40, 66]. Since α represents the ratio between the time scales of radial (transversal) diffusion $\tau_\mathrm{d} = a^2/D$ and longitudinal advection $\tau_\mathrm{s} = L/U$ (space time) we denote it here as normalized transverse diffusion time scale. A low Graetz number (respectively α) indicates that concentration profiles are well-developed (diffusion dominates), while high values mean the boundary layer is still developing (convection dominates). Values of the upper limit α_fd for which the exit concentration profile in laminar flow through a circular channel can be considered fully developed are $0.1063^{-1} \approx 9.4$ and $0.1021^{-1} \approx 9.8$ for kinetic and mass transfer control, respectively [66, Table 1]. A more conservative value corresponding to $\alpha_\mathrm{fd} = 2.5$ is given in [67].

Neglecting axial diffusion, Eq. (3) simplifies to

$$\frac{\partial C}{\partial \theta} + 2(1-R^2)\frac{\partial C}{\partial Z} = \frac{1}{\alpha}\frac{1}{R}\frac{\partial}{\partial R}\left(R\frac{\partial C}{\partial R}\right) - \frac{4}{\alpha}Da_\mathrm{b}C \tag{4}$$

In absence of a homogeneous reaction ($Da_\mathrm{b} = 0$), solutions of Eq. (4) depend on the single parameter α. Approximate analytical solutions of Eq. (4) for pulse-injection of a non-reactive passive tracer have been recently used to derive a model for the residence time distribution of laminar tubular flow in the transitional convection-diffusion regime of dispersion [68].

In this work, we are interested in steady solutions of the partial differential Eq. (4) only so that $C = C(R, Z)$. In this case, Eq. (4) simplifies to

$$2\alpha(1-R^2)\frac{\partial C}{\partial Z} = \frac{1}{R}\frac{\partial}{\partial R}\left(R\frac{\partial C}{\partial R}\right) - 4Da_\mathrm{b}C \tag{5}$$

The boundary conditions are as follows. The Dirichlet boundary condition at the inlet is

$$C = 1 \quad \text{at} \quad Z = 0, \quad 0 \leqslant R \leqslant 1 \tag{6}$$

The symmetry boundary condition at the axis of the tube is

$$\frac{\partial C}{\partial R} = 0 \quad \text{at} \quad R = 0, \quad 0 \leqslant Z \leqslant 1 \tag{7}$$

The first-order heterogenous reaction at the catalytic wall is implemented by means of the boundary condition

$$\frac{\partial C}{\partial R} = -Da_\mathrm{w} \cdot C \quad \text{at} \quad R = 1, \quad Z > 0 \tag{8}$$

which expresses the condition that the diffusion of the reacting species to the wall is equal to its removal by the heterogeneous reaction. Here,

$$Da_\mathrm{w} = \frac{\tau_\mathrm{d}}{\tau_\mathrm{r,w}} = \frac{k_\mathrm{w,obs} \cdot a}{D} = \frac{k_\mathrm{w,int} \cdot \eta \cdot a}{D} = \eta \cdot Da_\mathrm{II} \tag{9}$$

represents the effective Damköhler number for the heterogenous reaction. The effectiveness factor η has thus been included in the definition of Da_w, similar to [66]. In Eq. (9), $\tau_\mathrm{r,w} = a/k_\mathrm{w,obs}$ is the time scale of the heterogeneous reaction based on the observed (apparent) rate constant $k_\mathrm{w,obs} = \eta \cdot k_\mathrm{w,int}$, while $Da_\mathrm{II} = ak_\mathrm{w,int}/D$ is the (second) Damköhler number based on the intrinsic heterogeneous rate constant ($k_\mathrm{w,int}$). In the limits $Da_\mathrm{w} \to 0$ and $Da_\mathrm{w} \to \infty$, the Robin type wall boundary condition in Eq. (8) becomes of Neumann (uniform flux) and Dirichlet type (uniform zero concentration), respectively. It should be noted that for $Da_\mathrm{w} \neq 0$ the inlet condition (6) and the wall reaction condition (8) are mathematically not compatible at $Z = 0$, $R = 1$; therefore Eq. (8) applies for $Z > 0$. As a consequence, the radial concentration gradient at the wall is zero at $Z = 0$, but finite at $Z > 0$.

For the modeling of adsorption processes, $k_\mathrm{w,obs}$ in Eq. (9) could be replaced by the product of the molecular velocity of the reacting species in the radial direction following from kinetic gas theory ($\sqrt{R_\mathrm{g}T/2\pi M}$ where M is the molar mass of the diffusing gas) with a dimensionless parameter representing the fraction of collisions that lead to removal of the reacting species from the gas phase. For first order or pseudo-first order processes, this parameter is composed of a collection of constants including the sticking coefficient, as well as the rate constants for adsorption, desorption and surface reaction [69, pg. 771].

2.2.2 Formal Analytical and Early Numerical Solutions

The well-known formal analytical solution to Eqs. (5)–(8) for the case $Da_\mathrm{b} = 0$ is [70–72]

$$C(R, Z) = \sum_{i=1}^{\infty} A_i \cdot \varphi_i(R) \cdot \exp\left(-\frac{\lambda_i^2}{2\alpha}Z\right) \tag{10}$$

where λ_i is the i^{th} eigenvalue. The number of terms needed to obtain an accurate solution increase sharply as the inlet of the channel is approached ($Z \to 0$) or as convection becomes more dominant ($\alpha \to \infty$). In this case, the concentration profile can be obtained by Lévêque's solution, a simplified treatment concerned with the thin boundary layer that develops near the wall in the entry region. In the other limit when the concentration profile is fully developed, retaining only one term from the series in Eq. (10) is enough (one-term Graetz regime) [72]. Averaging Eq. (10) over the channel cross-section, with the velocity profile, yields for the axial profile of the mixing-cup concentration the result

$$C_{\text{cup}}(Z) = \sum_{i=1}^{\infty} w_i \cdot \exp\left(-\frac{\lambda_i^2}{2\alpha} Z\right) \tag{11}$$

where the coefficients w_i include integration constants and eigenfunction derivatives at the wall and fulfill the summation condition $\sum w_i = 1$.

First numerical solutions of Eqs. (5)–(6) for laminar tube flow with a first order homogeneous reaction ($Da_{\text{b}} > 0,\ Da_{\text{w}} = 0$) are presented in [73], and in combination with heat transfer in [74]. For a first order catalytic reaction at the tube wall ($Da_{\text{w}} > 0,\ Da_{\text{b}} = 0$) early numerical solutions of an equivalent form of Eq. (5) obtained by different normalization are presented in [75]. Concurrent first-order homogeneous and heterogeneous reactions in Poiseuille flow, including axial and radial diffusion, were investigated by Walker [76]; he obtained an infinite series of ordinary differential equations and computed roots of the Bessel function numerically.

2.2.3 Regimes

The present dimensional problem is characterized by four time scales ($\tau_{\text{d}},\ \tau_{\text{s}},\ \tau_{\text{r,b}}, \tau_{\text{r,w}}$). A large time scale means that the respective process is slow, while a small time scale means that the process is fast. From the four time scales, three independent non-dimensional groups (α, Da_{b}, Da_{w}) representing time scale ratios have been defined. Solutions of the boundary value problem in Eqs. (5)–(8) depend on α, Da_{w} and Da_{b} only. For the case $Da_{\text{b}} = 0$ we are left with three time scales ($\tau_{\text{d}}, \tau_{\text{s}},\ \tau_{\text{r,w}}$). In the kinetically controlled regime, the time scale of transverse diffusion is small as compared to both, the time scale of the heterogeneous reaction and the space time ($Da_{\text{w}} = \tau_{\text{d}}/\tau_{\text{r,w}} \ll 1,\ \alpha = \tau_{\text{d}}/\tau_{\text{s}} \ll 1$). In the kinetic regime, the reaction causes no substantial concentration gradient across the pipe outlet. In the Graetz regime, the time scale of transverse diffusion is small as compared to the space time ($\alpha = \tau_{\text{d}}/\tau_{\text{s}} \ll 1$) and the outlet concentration profile is fully developed. In the mass transfer controlled regime, the time scale of transverse diffusion is large as compared to the mean residence time ($\alpha = \tau_{\text{d}}/\tau_{\text{s}} \gg 1$) while at the same time the time scale of transverse diffusion is large as compared to the time scale of the heterogeneous reaction ($Da_{\text{w}} = \tau_{\text{d}}/\tau_{\text{r,w}} \gg 1$). In this limiting case a pronounced concentration boundary layer occurs, where the wall concentration is zero while the concentration in the pipe center is uniform at inlet value (Lévêque regime; $\alpha\ , Da_{\text{w}} \gg 1$). Lastly, mass transfer and kinetics are both limiting when the typical times scales are similar ($\alpha\ , Da_w \approx 1$).

3 Novel Approximate One-term Conversion Model

This section presents the novel approximate solution for the non-dimensional reactant mass balance equation which is then used to derive a one-term approximation for the end-of-pipe (exit) concentration and overall conversion. By separation of variables, the governing PDE is transferred to two ODEs, one describing the dependence on the axial and one on the radial co-ordinate. For the solution of the radial ODE, an ansatz is made which fulfills the boundary conditions; the eigenvalue follows from the condition that the ansatz fulfills the ODE. This is in contrast to the Sturm-Liouville approach, where the eigenvalues of a set of orthogonal eigenfunctions are obtained by matching the solution of the radial ODE with the boundary conditions.

3.1 Ansatz for Local Concentration Field

By separation of variables, the partial differential Eq. (5) can be reduced to a pair of ordinary differential equations. To this end the solution will be sought in terms of the product of two independent functions, one a function of R alone and the second a function of Z alone,

$$C(R, Z) = K \cdot \varphi(R) \cdot \psi(Z) \tag{12}$$

with pre-factor K being independent on R and Z. By ansatz (12), the concentration field is represented by one single term. This is in contrast to the analytical solution (10), where the concentration field is obtained by summation over the eigenmodes and coefficients A_i are chosen to fulfill the inlet condition Eq. (6). As will be shown below, the ansatz in Eq. (12) does not allow the inlet condition according to Eq. (6) to be satisfied exactly, but only approximately. The validity of the derived one-term expression for the exit concentration (and conversion) will thereby be inherently limited (to the Graetz regime) as discussed below.

Substituting Eq. (12) into Eq. (5), multiplying by α/K and separating the functions $\varphi(R)$ and $\psi(Z)$ yields

$$\alpha\frac{\psi'(Z)}{\psi(Z)} = \frac{\varphi''(R)+\varphi'(R)/R-4D\alpha_b\cdot\varphi(R)}{2(1-R^2)\cdot\varphi(R)} \tag{13}$$

Here, the prime marks indicate differentiation with respect to the independent variable. Each side of Eq. (13) must be equal to a common constant which is chosen as -2ω where $\omega > 0$. This yields two ordinary differential equations that are coupled via the constant ω (referred to as an eigenvalue). The first ODE describing the dependence on the axial coordinate is

$$\psi'(Z)+\frac{2\omega}{\alpha}\psi(Z)=0 \tag{14}$$

Integration of Eq. (14) and setting the integration constant to zero so that $\psi(Z=0)=1$ yields

$$\psi(Z|\alpha)=\exp\left(-\frac{2\omega Z}{\alpha}\right) \tag{15}$$

Substituting Eq. (15) into Eq. (12) gives

$$C(R,Z|\alpha)=K\cdot\varphi(R)\cdot\exp\left(-\frac{2\omega Z}{\alpha}\right) \tag{16}$$

where $\varphi(R)$, ω and K are unknown so far.

3.2 Eigenvalue Equation

The second-order ODE for the radial function $\varphi(R)$ resulting from Eq. (13) is

$$\varphi''(R)+\frac{1}{R}\varphi'(R)+4\left[\omega(1-R^2)-Da_b\right]\varphi(R)=0 \tag{17}$$

This equation corresponds to [55, Eq. 2.9] and reduces for $Da_b=0$ to [77, Eq. 3]. Lauwerier [78] presented two special solutions and denoted them as Poiseuille functions, in view of their importance in problems connected with Poiseuille flow in cylindrical tubes. The ODE in Eq. (17) is of confluent hypergeometric type and its general solution is the confluent (Kummer's) hypergeometric function.

The boundary conditions for Eq. (17) following from Eq. (7) and Eq. (8) are

$$\varphi'(R=0)=0 \tag{18}$$

and

$$\varphi'(R=1)=-Da_w\cdot\varphi(R=1) \tag{19}$$

To solve Eq. (17) with the latter boundary conditions for the case without heterogeneous reaction ($Da_w=0$), Lauwerier [55] made the following ansatz for the radial eigenfunctions

$$\varphi(R)=\sum_{k=0}^{\infty}b_k^*R^{2k} \tag{20}$$

where $b_0^*=1$. Further coefficients are determined by substituting the ansatz in Eq. (20) into Eq. (17) and collecting terms of power R^{2k-2}. Satisfying the ODE requires $b_1^*=-(\omega-Da_b)$ while further coefficients can be calculated from the recurrence relation

$$b_k^*=\frac{\omega b_{k-2}^*-(\omega-Da_b)b_{k-1}^*}{k^2},\quad k\geqslant 2 \tag{21}$$

In the approach of Lauwerier [55], the boundary condition in Eq. (19) gives in combination with $Da_w=0$ the eigenvalue equation.

$$\sum_{k=1}^{\infty}k\cdot b_k^*=0 \tag{22}$$

from which a set of real and positive eigenvalues ω_1, ω_2, $\omega_3\ldots$ can be derived.

In this work, we are interested in tubular flow with heterogeneous reaction ($Da_w>0$). Analytical results for this case using an ansatz similar to Eq. (20) have been obtained in [79]. In this paper, we combine the above approach of Lauwerier [55] for a homogeneous reaction with an ansatz used by Nigam et al. [80] for combined first-order homogeneous-heterogeneous reactions. By applying the Galerkin method in the Laplace transform domain and considering the sequence of functions

$$f_k(R|Da_w)=1-\frac{Da_w}{2k+Da_w}R^{2k},\quad k=1,2,3,\ldots \tag{23}$$

a closed-form analytical solution of the problem was obtained [80]. Each function of the infinite sequence in Eq. (23) satisfies the boundary conditions in Eq. (18) and Eq. (19), is twice continuously differentiable over the domain $0\leq R\leq 1$, and any finite set of the functions is linearly independent over the domain. Motivated by these features, we search in this paper a solution for Eq. (17) of the form

$$\begin{aligned}\varphi(R|Da_\mathrm{w}) &= \sum_{k=1}^{\infty} b_k \cdot f_k(R|Da_\mathrm{w}) \\ &= \sum_{k=1}^{\infty} b_k - Da_\mathrm{w} \sum_{k=1}^{\infty} \tfrac{b_k R^{2k}}{2k+Da_\mathrm{w}}\end{aligned} \tag{24}$$

By this ansatz which requires $Da_\mathrm{w} > 0$, the boundary conditions in Eq. (18) and Eq. (19) are automatically fulfilled. However, it should be noted that the functions f_k in Eq. (23) do not fulfill Eq. (17) even in the case $Da_\mathrm{b} = 0$, and are thus not eigenfunctions of the ODE.

To determine the coefficients b_k we substitute the ansatz in Eq. (24) back to Eq. (17), which yields

$$\begin{aligned}&\left[\omega(1-R^2) - Da_b\right] \sum_{k=1}^{\infty} b_k \\ &-Da_w \sum_{k=1}^{\infty} \tfrac{b_k}{2k+Da_w} \left[k^2 R^{2k-2} + (\omega - Da_b) R^{2k} - \omega R^{2k+2}\right] = 0\end{aligned} \tag{25}$$

Collecting terms of power R^{2k-2} in Eq. (25) indicates (see Supplemental Material) that terms of higher order than R^2 can be eliminated by setting

$$b_k = \frac{2k+Da_\mathrm{w}}{k^2}\left(\frac{b_{k-2}\omega}{2(k-2)+Da_\mathrm{w}} - \frac{b_{k-1}(\omega - Da_\mathrm{b})}{2(k-1)+Da_\mathrm{w}}\right), \quad k \geqslant 3 \tag{26}$$

By making use of the recurrence relation in Eq. (26), Eq. (25) simplifies to the form

$$\begin{aligned}&\left(-b_1 \tfrac{Da_w}{2+Da_w} + (\omega - Da_b) \sum_{k=1}^{\infty} b_k\right) \cdot R^0 \\ &- \left(b_1 \tfrac{(\omega - Da_b) Da_w}{2+Da_w} + b_2 \tfrac{4Da_w}{4+Da_w} + \omega \sum_{k=1}^{\infty} b_k\right) \cdot R^2 = 0\end{aligned} \tag{27}$$

At this stage, only b_1, b_2 and ω are left as free parameters. In order to fulfill Eq. (27) we bring it in a form which allows eliminating the dependance on R^2. This is achieved by defining

$$b_2 = -\frac{b_1}{4}\frac{4+Da_\mathrm{w}}{2+Da_\mathrm{w}}\frac{\omega + \omega^2 + Da_\mathrm{b}(Da_\mathrm{b} - 2\omega)}{\omega - Da_\mathrm{b}} \tag{28}$$

Substituting Eq. (28) into Eq. (27) gives

$$\begin{aligned}&\left(\tfrac{Da_\mathrm{w}}{2+Da_\mathrm{w}} \cdot b_1 - (\omega - Da_\mathrm{b}) \cdot \sum_{k=1}^{\infty} b_k\right) \\ &\cdot \left(1 - \tfrac{\omega}{\omega - Da_\mathrm{b}} R^2\right) = 0\end{aligned} \tag{29}$$

To satisfy Eq. (29), the expression in the first set of parentheses must be zero, which yields the condition

$$Da_\mathrm{w} - (2+Da_\mathrm{w})(\omega - Da_\mathrm{b}) \cdot \sum_{k=1}^{\infty} \frac{b_k}{b_1} = 0 \tag{30}$$

in combination with $\omega \neq Da_\mathrm{b}$. Equation (30) serves as eigenvalue equation from which for each combination of Da_w and Da_b the eigenvalue $\omega = \omega(Da_\mathrm{w}, Da_\mathrm{b})$ is determined. By Eq. (28) and Eq. (26), the coefficients b_k for $k \geq 2$ are linear proportional to b_1. Since it is only the ratio b_k/b_1 that enters into Eq. (30), the eigenvalue ω is independent on the specific choice for the sole remaining free parameter b_1. For simplicity we set $b_1 = 1$. The coefficients $b_k(Da_\mathrm{w}, Da_\mathrm{b}, \omega)$ for $k = 2 \cdots 5$ are listed in Appendix A, see Supplemental Material.

We now use Eq. (30) to replace the first infinite sum on the right-hand-side of Eq. (24) so that

$$\begin{aligned}&\varphi(R|Da_\mathrm{w}, Da_\mathrm{b}, \omega) \\ &= \tfrac{Da_\mathrm{w}}{(2+Da_\mathrm{w})(\omega - Da_\mathrm{b})} - Da_\mathrm{w} \sum_{k=1}^{\infty} \tfrac{b_k R^{2k}}{2k+Da_\mathrm{w}}\end{aligned} \tag{31}$$

In view of Eq. (16) we now define the normalized function $\Phi(R) = K \cdot \varphi(R)$ and set $K = 1/\varphi(R=0) = (2+Da_\mathrm{w})(\omega - Da_\mathrm{b})/Da_\mathrm{w}$ so that

$$\begin{aligned}&\Phi(R|Da_\mathrm{w}, Da_\mathrm{b}, \omega) \\ &= 1 - (2+Da_\mathrm{w})(\omega - Da_\mathrm{b}) \sum_{k=1}^{\infty} \tfrac{b_k(Da_\mathrm{w}, Da_\mathrm{b}, \omega)}{2k+Da_\mathrm{w}} R^{2k}\end{aligned} \tag{32}$$

and $\Phi(R=0) = 1$. The functions φ and Φ in Eq. (31) and Eq. (32) are − in combination with ω determined from Eq. (30) − solutions of Eq. (17) with boundary conditions in Eq. (18) and Eq. (19). However, it should be noted that each individual term of the summation series does not represent a solution of the ODE in Eq. (17). Individual terms of the series are therefore not eigenfunctions of the ODE.

3.3 Series truncation

For practical computations, the infinite sums in Eq. (30) and Eq. (32) must be truncated. To this end we replace the upper summation limit in both equations by integer parameter $m \geq 1$. As m^{th} order approximation of the eigenvalue Eq. (30) we define

$$\begin{aligned}&Da_\mathrm{w} - (2+Da_\mathrm{w})(\omega_m - Da_\mathrm{b}) \\ &\cdot \sum_{k=1}^{m} b_k(Da_\mathrm{b}, Da_\mathrm{w}, \omega_m) = 0\end{aligned} \tag{33}$$

Equation (33) yields a polynomial in ω_m of order m with coefficients depending on Da_w and Da_b. The eigenvalue $\omega_m = \omega_m(Da_\mathrm{b}, Da_\mathrm{w})$ for any approximation order is chosen as the lowest real root of the polynomial. Figure 1 compares the first five eigenvalues. For $m = 2$ and $m = 4$ real roots exist only for a limited region of the $Da_\mathrm{w} - Da_\mathrm{b}$ plane where Da_b is sufficiently low, whereas for odd

values of m there exists always one real root in the entire $Da_\mathrm{w} - Da_\mathrm{b}$ plane. For $Da_\mathrm{b} < 0.5$ the difference between ω_3, ω_4 and ω_5 is small while the difference between ω_3 and ω_5 increases with increase of Da_b. In the following, we consider odd values of m only. It is $\omega_1 < \omega_3 < \omega_5 < \cdots$ with $\omega_m\,(Da_\mathrm{w}, Da_\mathrm{b}) > Da_\mathrm{b}$, see Fig. 2.

The radial function associated with the approximation order m is

$$\begin{aligned}&\Phi_m(R|Da_\mathrm{b},\omega_m)\\ &= 1-(2+Da_\mathrm{w})(\omega_m - Da_\mathrm{b})\sum_{k=1}^{m}\frac{b_k(Da_\mathrm{w},Da_\mathrm{b},\omega_m)}{2k+Da_\mathrm{w}}R^{2k}\end{aligned} \tag{34}$$

with the residual of the radial ODE being of order R^{2m}. The first three approximations of this function can be represented as

$$\underbrace{\underbrace{\underbrace{-R^2}_{m=1}+\frac{1}{4}\frac{\omega(1+\omega)+Da_b(Da_b-2\omega)}{\omega-Da_b}R^4}_{m=2}-\frac{\omega(\omega+5)+Da_b(Da_b-2\omega)}{36}R^6}_{m=3} \tag{35}$$

where ω has to be taken as ω_m with m equal to 1, 2, or 3, respectively. For $Da_b = 0$, we give in Eq. (36) the approximation for $m = 5$ which will be used below

$$\begin{aligned}\frac{\Phi_{5,Da_b=0}(R|\omega)-1}{\omega} &= -R^2+\frac{1+\omega}{4}R^4-\frac{\omega(5+\omega)}{36}R^6\\ &+\frac{\omega(9+14\omega+\omega^2)}{576}R^8-\frac{\omega^2(89+30\omega+\omega^2)}{14\,400}R^{10}\end{aligned} \tag{36}$$

The numbers in the denominators on the right-hand-side of Eq. (36) correspond to $(2!)^2$, $(3!)^2$, $(4!)^2$ and $(5!)^2$ so that good convergence is to be expected.

3.4 Local Concentration Field

From each normalized truncated function Φ_m given by Eq. (34) and the associated truncated eigenvalue ω_m determined by Eq. (33) we now define the truncated concentration field

$$C_m(R,Z|\alpha,\omega_m) = K_m\cdot\Phi_m(R|\omega_m)\cdot\exp\left(-2\omega_m Z/\alpha\right) \tag{37}$$

representing an approximate solution of Eq. (17) with radial boundary conditions in Eq. (18) and Eq. (19). The approximate concentration field at the inlet ($Z = 0$) is

$$C_m(R,Z=0|\alpha,\omega_m) = K_m\cdot\Phi_m(R|\omega_m) \tag{38}$$

Because $\omega_m(Da_\mathrm{w}, Da_\mathrm{b}) > Da_\mathrm{b}$ it is evident from Eq. (34) that Φ_m cannot be independent on R. Thus, $C_m(R, Z = 0)$ does not fulfill the inlet condition of radially uniform concentration as given by Eq. (6).

To illustrate the local concentration field, we consider the case $Da_\mathrm{b} = 0$ in combination with $K_m = 1$. Of special relevance are the third and fifth approximation orders. Figure 3 compares the approximate concentration field $C_5(R, Z)$ with the numerical solution of the PDE by the computer program Mathematica (C_num) for $\alpha = 1$, $Da_\mathrm{w} = 0.5$, $Da_\mathrm{b} = 0$. For

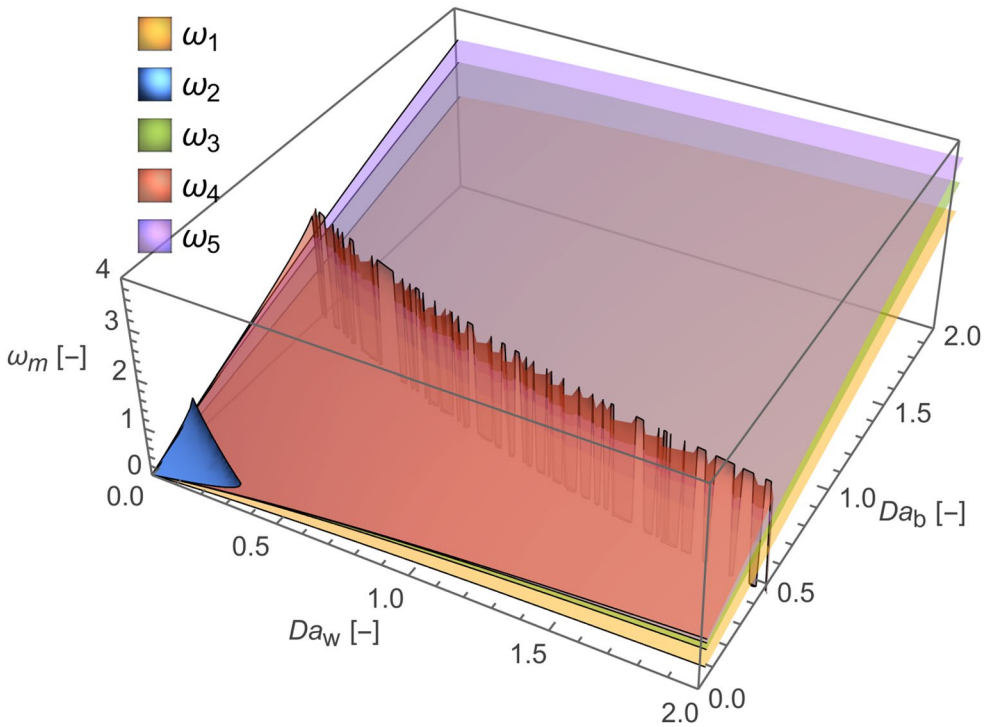

Fig. 1 Comparison of first five eigenvalues. Eigenvalue approximations ω_1 and ω_3 are evaluated analytically while the other ones are evaluated numerically

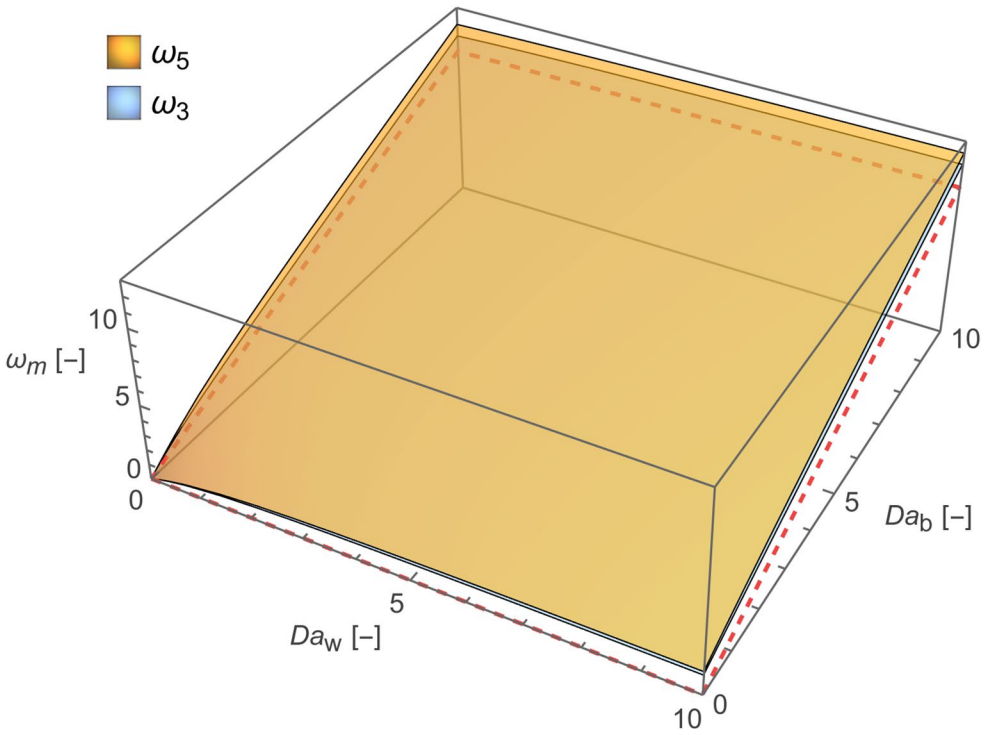

Fig. 2 3D plot of eigenvalues $w_3(Da_\mathrm{w}, Da_\mathrm{b})$ and $w_5(Da_\mathrm{w}, Da_\mathrm{b})$. The dashed red line shows the plane corresponding to $\omega = Da_\mathrm{b}$ for comparison

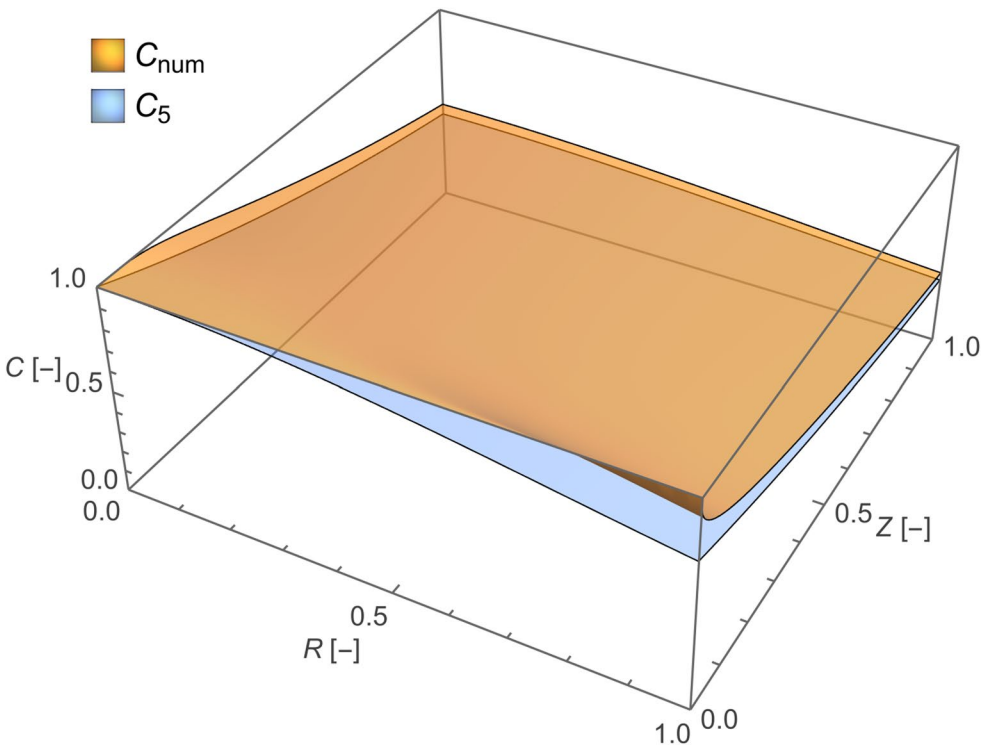

Fig. 3 Comparison of approximate concentration field $C_5(R, Z)$ with the numerical solution of the PDE by computer program Mathematica (C_num) for $\alpha = 1$, $Da_\mathrm{w} = 0.5$, $Da_\mathrm{b} = 0$

$R = Z = 0$ it is $C_\mathrm{num} = C_5 = 1$ whereas in the rest of the channel it is $C_\mathrm{num} > C_5$. At the inlet ($Z = 0$), the numerical concentration is 1 as specified; the concentration C_5 is instead not radially uniform, as expected. The difference between both concentration fields is largest at ($Z = 0$, $R = 1$). For a fixed radial position, both concentration fields decrease with increase of Z. The axial gradient of C_num at ($R = 1$, $Z = 0$) is very large. This may be attributed to the incompatibility of the inlet condition and the reactive wall boundary condition mentioned above. The differences between C_5 and C_num decrease with increase of Z and are very small at the outlet. We conclude that C_5 is not a good approximation to

the numerical solution for small values of Z but is reasonably accurate for large values of Z. In this paper, we are not interested in a highly accurate solution of the concentration field within the tubular channel but in a reasonably accurate approximation of the conversion which is determined by the outlet concentration profile.

3.5 End-of-pipe Concentration

Of greatest practical interest is the mixing-cup concentration of the reactant at any axial position in the tube, particularly at the outlet. It is obtained by integrating the local concentration in Eq. (37) over the pipe cross-section taking into account the radially varying axial velocity, i.e.

$$\begin{aligned}\overline{C}_m(Z) &= 4\int_0^1 C_m(R,Z)\cdot(1-R^2)\cdot \mathrm{d}R \\ &= K_m\cdot\exp\left(-\tfrac{2\omega_m Z}{\alpha}\right)\cdot \underbrace{4\int_0^1 R(1-R^2)\cdot\Phi_m(R|\omega_m)\cdot \mathrm{d}R}_{=\Phi_{cup,m}}\end{aligned} \tag{39}$$

Inserting Φ_m from Eq. (34) into Eq. (39) and performing the integration yields

$$\begin{aligned}\Phi_{\mathrm{cup},m}(Da_\mathrm{w}, Da_\mathrm{b}, \omega_m) &= 1-2(\omega_m - Da_\mathrm{b}) \\ &\cdot\sum_{k=1}^{m}\tfrac{2+Da_\mathrm{w}}{2k+Da_\mathrm{w}}\tfrac{b_k(Da_\mathrm{w},Da_\mathrm{b},\omega_m)}{(k+1)(k+2)}\end{aligned} \tag{40}$$

To ensure that the inlet mixing-cup concentration $\bar{C}_m(Z=0)$ is 1 we require $K_m = 1/\Phi_{\mathrm{cup},m}$. The end-of-pipe concentration then takes the simple form

$$C_{\mathrm{eop},m}(\alpha,\omega_m) = \bar{C}_m(Z=1) = \exp\left(-\frac{2\omega_m}{\alpha}\right) \tag{41}$$

where $\omega_m = \omega_m(Da_\mathrm{w}, Da_\mathrm{b})$. In a logarithmic plot of $C_{\mathrm{eop},m}$ versus $1/\alpha$, Eq. (41) is a straight line with slope $-2\omega_m/\alpha$.

For a first test of the accuracy of the one-term model in Eq. (41), we compare the approximate end-of-pipe concentrations $C_{\mathrm{eop},3}$ and $C_{\mathrm{eop},5}$ for $Da_\mathrm{b}=0$ with that determined from the exact (numerical) solution of the PDE system and with the one-term approximation of Lopes et al. [40, 41] for a first order reaction. In the present notation, the exit mixing-cup concentration for laminar flow laminar flow through a circular channel of the LRC model [40, Eqs. 11 and 14] is given by

$$C_{\mathrm{eop,LRC}}(\alpha, Da_\mathrm{w}) = w_1\cdot\exp\left(-\frac{Da_\mathrm{w}}{1+2\frac{Da_\mathrm{w}}{Sh_\infty}}\frac{2}{\alpha}\right) \tag{42}$$

where $Sh_\infty = 3.6568$ is the external asymptotic Sherwood number (based on pipe diameter) in the Dirichlet limit $Da_\mathrm{w}\to\infty$ (zero wall concentration). In Eq. (42), w_1 is the first Fourier weight [81] which is modelled as

$$w_1 = w_{1.\infty} + \frac{1-w_{1.\infty}}{1+\frac{1-w_{1.\infty}}{w_{1.\infty}}Da_\mathrm{w}} \tag{43}$$

where $w_{1,\infty} = 0.8191$. The external asymptotic Sherwood number depends only on the geometric shape of the flow channel and is tabulated for various standard flow geometries [81, 82].

Adopting the graphical representation from [75], we plot in Fig. 4 the end-of-pipe concentration versus $1/\alpha$ for six different values of Da_w and the first three odd approximations orders. Approximation order $m=1$ considerably overestimates the numerical end-of-pipe concentration and is not considered further here. For $Da_\mathrm{w}=0.1$, the difference between approximation orders $m=3$ and $m=5$ is very small and the agreement with the numerical result is very good. For larger values of Da_w, the difference between approximation orders $m=3$ and $m=5$ is larger. As is to be expected, the difference between the present model and the numerical data is smaller for $m=5$ as compared to $m=3$ while the end-of-pipe concentration of the LRC model is mostly in between but close to $C_{\mathrm{eop},5}$. A quantitative estimation of the error of the present approximation is given below.

3.6 Conversion

By Eq. (41) and with $\omega_m = \omega_m(Da_\mathrm{w}, Da_\mathrm{b})$ the conversion becomes

$$X_m(\alpha, Da_\mathrm{w}, Da_\mathrm{b}) = 1 - C_{\mathrm{eop},m} = 1-\exp\left(-\frac{2\omega_m}{\alpha}\right) \tag{44}$$

The present model for the conversion thus requires only the approximate eigenvalue ω_m but not the function Φ_m. Figures 1 and 2 show that for odd values of m the approximate eigenvalue ω_m increases with m. Therefore, $C_{\mathrm{eop},m}$ decreases with increase of odd m (Fig. 4) while conversion X_m increases with increase of odd m. Hence, conversion predicted by a lower odd approximation order m is conservative in the sense that overall conversion is underpredicted as compared to higher odd approximation order.

The approximation X_1 − which is obtained by inserting ω_1 given in Eq. (B.1) into Eq. (44) − cannot be recommend given the large deviations of $C_{\mathrm{eop},1}$ from the numerical solution (cf. Figure 4). The eigenvalue equations for $m=3$ and $m=5$ are given in Appendix B, see Supplemental Material.

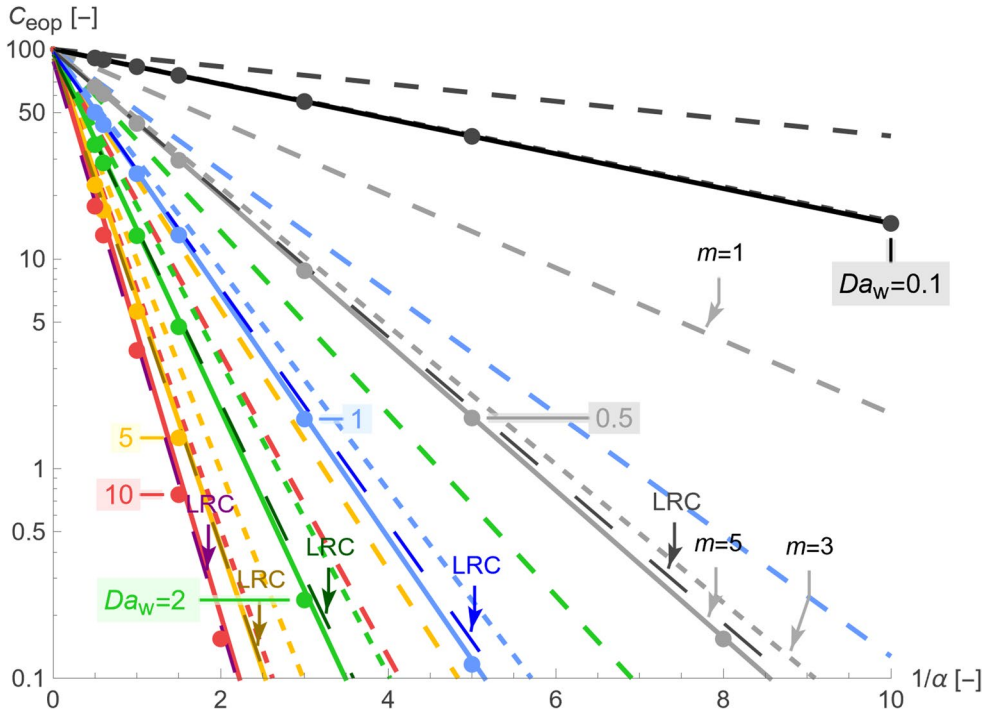

Fig. 4 Normalized end-of-pipe concentration in absence of a homogeneous reaction ($Da_b = 0$) versus $1/\alpha$ for six different values of the heterogeneous Damköhler number Da_w (distinguished by color). Symbols (dots) represent numerical results by computer program Mathematica. Thick lines represent end-of-pipe concentration predicted by the present analytical model for different approximation orders (long-dashed lines $m = 1$, short-dashed lines $m = 3$, solid lines $m = 5$). Thin long-dashed lines represent the LRC model [40] given by Eqs. (42) and (43)

The eigenvalue ω_3 is the root of a cubic equation and can be calculated directly, see Eq. (B.3) in the Supplemental Material. Determining ω_5 as the root of fifth order polynomial (B.7) requires a numerical solution instead. Before we quantify the accuracy of both approximations, we first discuss the limiting behavior of Eq. (44).

In the limit $\alpha \to 1$ we have $X_m \to 1$ independent on the values of Da_w and Da_b. In the limit $Da_w \to 0$ the function φ in Eq. (24) becomes independent on R. In this case, the local concentration field at any axial position of the tube is radially uniform. The respective limit of the eigenvalue ω_m for $m = 3,\ 5,\ 7, \cdots$ is $\omega_m \to 2Da_b$ (see Supplemental Material Fig. SM-1). The conversion in Eq. (44) then becomes

$$X_{Da_w \to 0} = 1 - \exp\left(-\frac{4Da_b}{\alpha}\right) = 1 - \exp\left(-k_b \tau_s\right) \qquad (45)$$

where $\tau_s = L/U = V/Q$ is the space time. This result agrees with the conversion by a first-order irreversible reaction in an ideal plug flow reactor with uniform velocity and no axial mixing.

For most commercially important reactor problems, if the temperatures are high enough for the homogeneous reaction to proceed rapidly, the heterogeneous reaction is of little consequence; conversely, if the temperatures are in a range in which the catalytic wall reaction is important, the homogeneous reaction does not usually proceed perceptively [83]. Here, we are mainly interested in heterogeneous reactions and restrict the following analysis to the case without homogeneous reaction ($Da_b = 0$).

Figure 5 compares – for the case $Da_b = 0$ – the conversion predicted by present model X_5 (color lines) with numerically computed conversion (symbols) for a wide parameter range covering five orders of magnitude in α and four orders of magnitude in Da_w. While deviations are small provided $\alpha \le 1$ or $Da_w \le 0.1$, they increase with increase of either parameter. For $\alpha \ge 10$ and $Da_w \ge 1$ the deviation becomes very large resulting in a large relative error of X_5 as discussed below. Figure 5 also compares the limiting behavior of the present model with known limits of the exact analytical solution [44, Sect. 3.4] where $P = \alpha/4$ and $\phi_s^2 = Da_w/2$. In the limit $Da_w \to 0$ we have $\omega_m \to Da_w$ (see Fig. SM-2 in Supplemental Material) so that Eq. (44) yields $X_m \to 1 - \exp(-2Da_w/\alpha)$ for $m = 3,\ 5,\ 7, \cdots$. For $\alpha \ll 1$, the latter expression can be approximated as $X_{m,0} = 2Da_w/\alpha$ in agreement with the exact analytical limit of the kinetic regime [44, Eq. 35]. In the Dirichlet limit $Da_w \to \infty$ we have $\omega_m \to 1.828$ for large odd m (see Fig. SM-3 in Supplemental Material) so that $X_{m,\infty} \to 1 - \exp(-3.656/\alpha)$ in this limit, where the numerical value in the exponent is one half of the first eigenvalue $\lambda_{1,\infty}^2 = 7.313$ in the Dirichlet limit (see e.g. [72, Eq. 6b]). Figure 5 shows that $X_{m,\infty}$ notably underestimates the numerical conversion when both Da_w and α are large and strongly deviates from the analytical limit for the mass transfer controlled regime where $X = 2.563/\alpha^{2/3}$ [44, Eq. 34b].

To quantify the error of the present conversion model, we plot in Fig. 6 the relative error $\epsilon_m = (X_{num} - X_m)/X_{num}$ in comparison to the numerical conversion (X_{num}) as

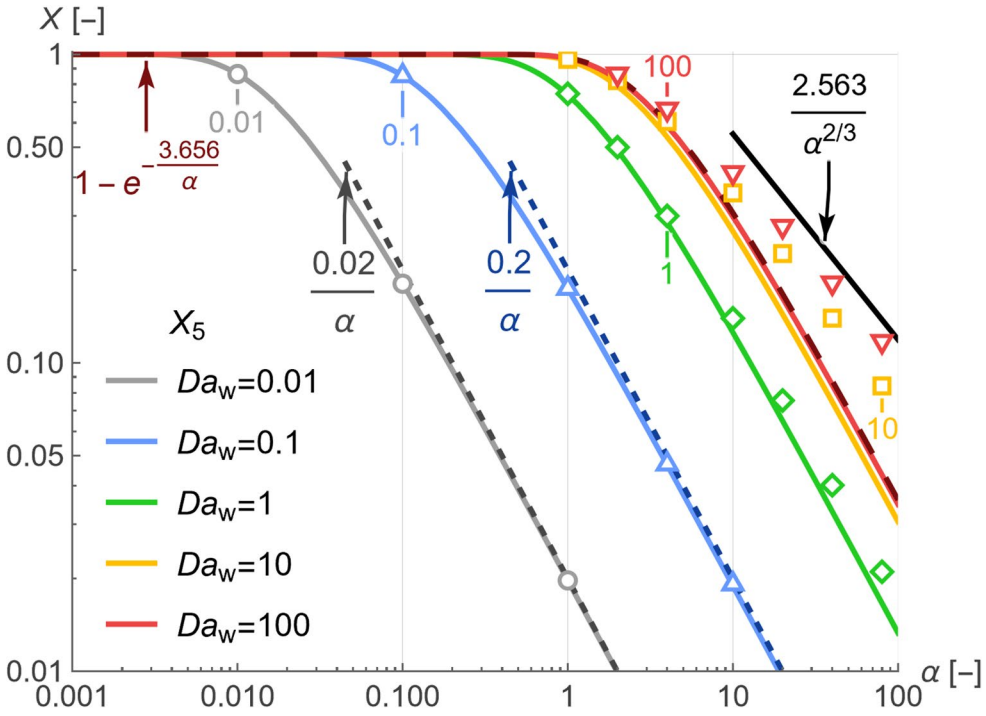

Fig. 5 Conversion versus α for $Da_{\mathrm{b}} = 0$. Solid lines show X_5 for five different values of Da_{w}. Open symbols show numerical results for the five values of Da_{w} and selected values of α. Dashed lines show the limit of X_m for large values of m; short-dashed lines refer to the kinetically controlled regime ($Da_{\mathrm{w}} \ll 1$) where $X_{m,0} = 2Da_{\mathrm{w}}/\alpha$; the dark-red long-dashed line refers to the Dirichlet limit ($Da_{\mathrm{w}} \to \infty$). The black solid line in the upper right corner represents the analytical limit for the mass transfer controlled regime (α , $Da_{\mathrm{w}} \gg 1$) [44]

function of α for $m = 3$, 5, 7 and three different values of Da_{w}. For each value of Da_{w}, the error decreases with increase of m and decrease of α. While ϵ_3 is unacceptably large unless $\alpha \ll 1$, the error ϵ_5 is much smaller and only slightly larger than ϵ_7. From the analysis of the error ϵ_5 for other values of Da_{w} not shown in Fig. 6, an upper limit for α is derived as

$$\alpha \leqslant \mathrm{Min}\left(10,\ \mathrm{Max}\left(1,\ \frac{1+Da_{\mathrm{w}}}{2Da_{\mathrm{w}}}\right)\right) \tag{46}$$

so that $\epsilon_5 \leq 1\%$ while $\epsilon_3 \leq 6\%$. For $Da_{\mathrm{w}} \ll 1$, the upper limit of Eq. (46) is comparable to the value $\alpha_{\mathrm{fd}} \approx 2.5 - 10$ cited in Sect. 2.2.1, whereas for $Da_{\mathrm{w}} > 0.25$ it is lower. In conclusion, the approximation X_5 is in reasonably good

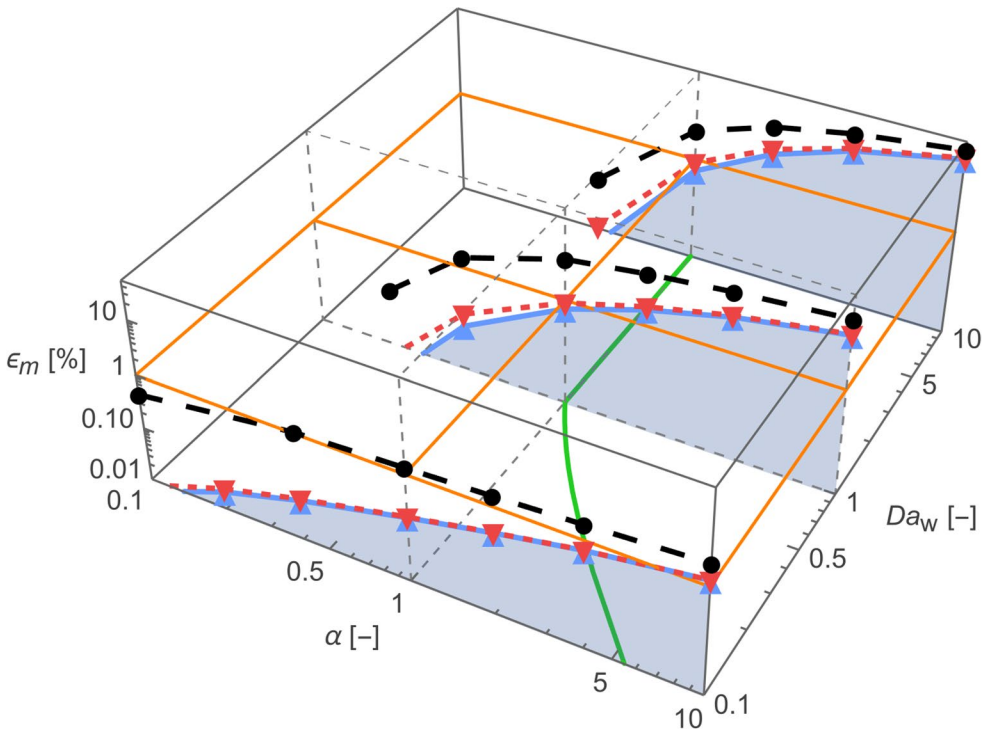

Fig. 6 Relative error $\epsilon_m = (X_{num} - X_m)/X_{num}$ for $m = 3$ (●), $m = 5$ (▼) $m = 7$ and (▲) as function of α for $Da_w = 0.1, 1, 10$ for $Da_b = 0$. The orange lines indicate an error of 1%. The green line at the plot bottom of the diagram represents the limit according to Eq. (46), such that $\epsilon_5 \leq 1\,\%$ holds

agreement with the numerical conversion when the criterion in Eq. (46) is respected, despite the deviations in the local concentration field (cf. Figure 3). While the accuracy of X_5 is notably higher, X_3 may nevertheless be advantageous for a quick conservative determination of conversion and light-off curves under parameter variations. For values of α larger than the upper limit in Eq. (46), the one-term representation of the ansatz in Eq. (12) is inappropriate and many eigenmodes are needed to accurately predict conversion [44].

Figure 7 shows a 3D plot of the present conversion model X_5 as function of the two parameters α and Da_w, both varied over three orders of magnitude from 0.01 to 10. A high conversion of almost 100% is obtained only in the region where $Da_\mathrm{w} = \tau_\mathrm{d}/\tau_\mathrm{r,w}$ is sufficiently high while $\alpha = \tau_\mathrm{d}/\tau_\mathrm{s}$ is sufficiently small. At large α, the time scale of radial diffusion $\tau_\mathrm{d} = a^2/D$ is large as compared to the time scale of longitudinal convection $\tau_\mathrm{s} = L/U$ (the space time). This means that during the passage of the gas stream through the tubular reactor, diffusion has insufficient time to transport reactive matter from the high-velocity region in the tube center to the wall. As a consequence, conversion is low regardless of the value of Da_w. The catalytic monolith is then operated under mass transfer limited conditions, i.e., the reactant species have insufficient time to diffuse to the wall and react before leaving the reactor. In the case of complete external mass transfer limitation, the concentration of the reactant at the channel wall is essentially zero. On the other hand, when α is small, the conversion can be low because the reaction is kinetically limited. In this case the time scale of the heterogeneous reaction $\tau_\mathrm{r,w} = a/k_\mathrm{w,obs}$ is large as compared to the time scale of radial diffusion $\tau_\mathrm{d} = a^2/D$ so that the Damköhler number $Da_\mathrm{w} = \tau_\mathrm{d}/\tau_\mathrm{r,w}$ is low.

3.7 Estimation of the Rate Constant

The present one-term conversion model can be used to determine from given experimental values of conversion X_exp and normalized transversal diffusion time scale α_exp the corresponding value of the apparent rate constant $k_\mathrm{w,obs}$. The procedure is as follows. With $X_m \approx X_\mathrm{exp}$ we obtain from Eq. (44) the relation

$$\omega_m(\alpha_\mathrm{exp}, X_\mathrm{exp}) = -\frac{\alpha_\mathrm{exp}}{2} \cdot \ln(1 - X_\mathrm{exp}) \tag{47}$$

For the case $Da_\mathrm{b} = 0$, one can derive from the truncated eigenvalue Eq. (33) for any value of m a relation of the form $Da_\mathrm{w} = Da_\mathrm{w}(\omega_m)$; the corresponding relations for $m = 3$ and $m = 5$ are given in the Appendix B in Eq. (B.6) and Eq. (B.9), see Supplemental Material. Taking into account that the argument in $Da_\mathrm{w}(\omega_m)$ can be expressed by Eq. (47), and incorporating the definition of Da_w in Eq. (9), we obtain

$$\begin{aligned} k_\mathrm{w,obs}\left(\alpha_\mathrm{exp}, X_\mathrm{exp}\right) &= \eta_\mathrm{exp} \cdot k_\mathrm{w,int}(\alpha_\mathrm{exp}, X_\mathrm{exp}) \\ &= \tfrac{D}{\alpha} \cdot Da_\mathrm{w}\left(\omega_m\left(\alpha_\mathrm{exp}, X_\mathrm{exp}\right)\right) \end{aligned} \tag{48}$$

4 Application to Ammonia SCR

In this section, the model developed in the previous section is applied to the selective catalytic reduction of NO. The present conversion model assumes steady state operation. This assumption is valid for stationary power plants [84] but not for automotive SCR. Only when the car is driving at constant speed, is the converter close to steady state [10].

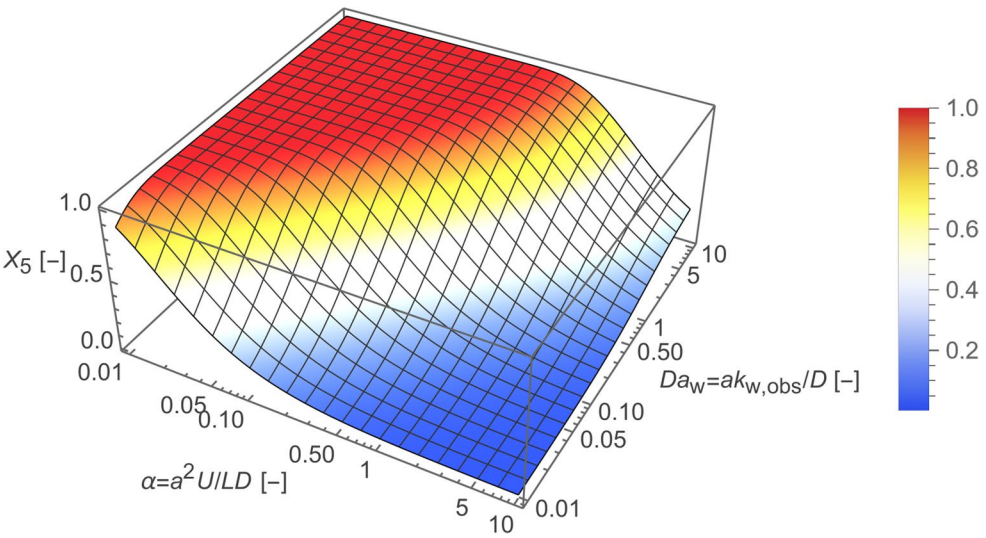

Fig. 7 3D plot of conversion by present model X_5 as function of the normalized transversal diffusion time scale α and the heterogeneous Damköhler number Da_w

The principal atmospheric pollutants present in automobile exhaust gas are carbon monoxide, a large variety of hydrocarbon species and nitrogen oxides (NO_x). In the urea-SCR process [85], the NO_x species (predominantly NO and NO_2) are reduced by injection of NH_3 to N_2 over a heterogeneous catalyst in the presence of O_2. The SCR reaction can be represented by six diffusion and reaction steps: (1) the NO and NH_3 reagents diffuse to the catalytic wall; (2) the reagents diffuse into the intraparticle surface of the catalyst via pore diffusion; (3) the reagents are adsorbed onto the catalytic surface; (4) the chemical reaction occurs on the catalytic surface; (5) the reaction product is desorbed from the intraparticle surface; and (6) the reaction product diffuses from the catalytic surface to the main flue gas stream [48]. The rate of the reaction is thus controlled by external and internal diffusion as well as chemical kinetic limitations.

In the previous section, physical properties of the gas are assumed constant as the present model is developed for isothermal conditions at a given temperature. The operating temperature of an SCR monolith may vary from less than 450 K (177 °C) at the cold start to more than 900 K (627 °C) at full load [86]. In this Section, we apply the conversion model X_5 for different values of the temperature. The reaction constants and the diffusion coefficient entering into the present model depend strongly on temperature. If we specify relationships for $k_{\mathrm{w,obs}}(T)$ and $D(T)$ and use the present model to estimate conversion at the channel outlet at various temperatures, we obtain a plot of conversion over temperature, commonly referred to as a light-off curve [87]. These curves allow comparison of different samples of catalysts under the same reaction conditions.

4.1 Kinetics and Diffusion Coefficient

A number of literature studies reported the mechanism of SCR reaction and it was shown that the SCR process can essentially proceed via three different pathways, depending on the ratio of NO and NO_2 in the feed [88]. Here we restrict our study to the most dominant reaction process

$$4\mathrm{NH_3} + 4\mathrm{NO} + \mathrm{O_2} \rightarrow 4\mathrm{N_2} + 6\mathrm{H_2O} \tag{49}$$

This reaction path, known as standard SCR, takes place when NO is the only NO_x species. For stoichiometric reaction, one mole of ammonia is required for each mole of NO. An important parameter for the SCR efficiency in technical applications is therefore the inlet NH_3/NO molar ratio.

Several studies assume Eley-Rideal kinetics for the SCR [23, 48, 89, 90]. That is, NH_3 molecules are selectively adsorbed onto the catalytic surface and gaseous or weakly adsorbed NO_x molecules react with the strongly adsorbed NH_3 molecules. The reaction rate of NO is then expressed as

$$\dot{s}_{\mathrm{NO}} = k_{\mathrm{NO,obs}} \cdot C_{\mathrm{NO}} \cdot \underbrace{\frac{K_{\mathrm{NH_3}} C_{\mathrm{NH_3}}}{1 + K_{\mathrm{NH_3}} C_{\mathrm{NH_3}}}}_{\theta_{\mathrm{NH_3}}} \tag{50}$$

where $\theta_{\mathrm{NH_3}}$ is the fractional surface coverage of ammonia adsorbed on the active sites of the catalyst and $K_{\mathrm{NH_3}}$ is the (temperature dependent) adsorption constant of NH_3 gas. The value of $k_{\mathrm{NO,obs}}$ in Eq. (50) represents the overall rate constant for steps 2 to 5 as discussed above. Therefore, it is a combined effect of intrinsic chemical kinetic and intraparticle (pore) diffusion in the monolithic catalyst.

For NH_3/NO inlet molar ratios (β) of less than 1, increasing the ammonia injection quantity leads to better SCR performance, while for $\beta \geq 1$ the NH_3 concentration has almost no effect on the NO removal [89, 91, 92]. In this case, NO is the limiting reactant and the rate of the SCR reaction is first order with respect to NO and zero order with respect to NH_3 [39, 93, 94]. Already for a NH_3/NO feed ratio $\beta = 1$, the fractional surface coverage of adsorbed ammonia is close to unity [48, Table 3]. While the cited studies refer to vanadium-based catalysts, kinetic studies on Fe- and Cu-zeolite SCR catalysts also report an overall rate law that is approximately first-order in NO and zero-order in NH_3 for the standard SCR reaction under conditions where NH_3 coverage is high and nearly saturated [95–97]. Here we assume that active sites of the catalyst are completely covered by NH_3 ($\theta_{\mathrm{NH_3}} = 1$).

For the intrinsic rate constant $k_{\mathrm{NO,int}}$, we assume the familiar Arrhenius dependence on temperature so that Eq. (50) takes with $\theta_{\mathrm{NH_3}} = 1$ and $k_{\mathrm{NO,obs}} = \eta(T) \cdot k_{\mathrm{NO,int}}$ the form

$$\dot{s}_{\mathrm{NO}} = \eta(T) \cdot A_{\mathrm{NO}} \cdot \exp\left(-\frac{E_{\mathrm{NO}}}{R_{\mathrm{g}} T}\right) \cdot C_{\mathrm{NO}} \tag{51}$$

Here, A_{NO} is the pre-exponential factor, E_{NO} the catalytic activation energy, R_{g} the gas constant and T the absolute temperature. According to Eq. (51), NO reduction is independent of NH_3 concentration.

The temperature-dependence of the diffusion coefficient of gases is commonly described by a power law with exponent q between 1.5 and 2. Following Fuller et al. [98], we here use $q = 1.75$ and model the temperature-dependance of D as [9, 10]

$$\frac{D(T)}{D(T_0)} = \left(\frac{T}{T_0}\right)^{1.75} \tag{52}$$

where $D(T_0)$ denotes the diffusion coefficient at temperature T_0. The diffusion is approximated as binary NO in N_2 [39]. The binary diffusivity at standard temperature ($T_0 = 273.15\,\mathrm{K}$ and pressure $1\,\mathrm{atm}$) is taken as $D_{\mathrm{NO-N_2}}(T_0) = 1.809 \times 10^{-5}\,\mathrm{m^2/s}$ [99, Table 3]. With Eq. (51) and Eq. (52), the Damköhler number for the heterogeneous reaction defined in Eq. (9) becomes

$$Da_{\mathrm{NO}}(T) = \frac{a \cdot A_{\mathrm{NO}}}{D_{\mathrm{NO\text{-}N_2}}(T_0)} \cdot \eta(T) \cdot \left(\frac{T_0}{T}\right)^{1.75} \cdot \exp\left(-\frac{E_{\mathrm{NO}}}{R_{\mathrm{g}}T}\right) \tag{53}$$

exhibiting a rather complicated dependence on temperature. Due to the dependence of the diffusion coefficient on temperature, the normalized transversal diffusion time scale α is a function of temperature as well, see below.

4.2 Comparison with experimental data from literature

The experimental data of Buzanowski & Yang [39] and Beeckman & Hegedus [89] were chosen for comparison. For these studies, which both use V_2O_5-TiO_2 catalysts, rate constants with dimension m/s as required by the present model are reported. This is not the case for other catalyst materials. Both studies employ ceramic honeycomb monoliths with square shaped channels. The one-term conversion model presented in Sect. 3 is developed for circular channels. To apply the model to square channels, we use the theory of shape normalization for catalytic monoliths developed by Balakotaiah and coworkers [43, 44]. In this approach, the transport and reaction equations are rewritten so that different channel cross-sections, like square, triangular, circular, or more complex shapes, can be compared using the same dimensionless framework. Geometry is incorporated via shape-normalized length scales based on the surface area and perimeter at the fluid-washcoat interface; as a result, conversion behavior becomes nearly universal across different geometries, provided these scales are applied. If two monolith channels have different shapes but the same shape-normalized parameters, their mass-transfer and conversion trends are therefore very similar. According to the theory of shape normalization, the present model for a circular channel can be applied to a square channel provided the effective transverse diffusion length (R_Ω in [44]) is identical. For a circular channel it is $R_\Omega = a/2$, while for a square channel it is $R_\Omega = w/4$. In this Section, we therefore apply the present model with $a = w/2$.

The present model requires the mean velocity U as input parameter which is often not reported for catalytic monoliths. Instead, operational conditions of monolith converters are usually specified by the gas hourly space velocity $\mathrm{GHSV_{ref}}$ at a reference temperature (T_{ref}) and reference pressure (here $1\,\mathrm{atm}$). The GHSV is defined as the exhaust gas flow rate divided by the volume of the monolith. With the single channel model and assuming ideal gas behavior to account for thermal expansion it follows

$$\mathrm{GHSV}(T) = \mathrm{GHSV_{ref}} \cdot \frac{T}{T_{\mathrm{ref}}} = \mathrm{OFA} \cdot \frac{U(T)}{L} \tag{54}$$

Here, OFA denotes the open frontal area of the monolith (ratio between the monolith's free cross-section and the overall cross-section). OFA values of monoliths depend on the number of cells per square inch (CPSI) and the wall thickness; typical values are in the range $0.6 - 0.9$ [50, Fig. 6]. By Eq. (54), the GHSV is inversely proportional to space time $\tau_{\mathrm{s}}(T) = L/U(T)$, which represents the mean residence time of molecules in the gas stream at a given temperature. The temperature dependence of the normalized transversal diffusion time scale is then given by

$$\alpha(T) = \frac{a^2}{D(T)} \cdot \frac{U(T)}{L} = \frac{a^2}{D(T)} \cdot \frac{T}{T_{\mathrm{ref}}} \cdot \frac{\mathrm{GHSV_{ref}}/3600}{\mathrm{OFA}} \tag{55}$$

where the $\mathrm{GHSV_{ref}}$ is given in $\mathrm{h^{-1}}$.

4.2.1 Buzanowski and Yang

Buzanowski & Yang [39] presented theoretical and experimental results for the selective catalytic reduction of NO by NH_3 in a monolithic honeycomb reactor under power plant conditions. The authors derived a simple one-term exponential model that expresses the overall NO conversion as function of space velocity and other parameters (mass transfer coefficient, Thiele modulus, effective diffusivity in the pores of the washcoat) [39, Eq. 16]. The experiments were conducted in a monolith with 31 cells/cm^2 corresponding to 200 CPSI and an open frontal are of 0.578. Here we consider data of [39], Table III where the overall conversion of NO over 3.45 wt% V_2O_5/TiO_2 catalyst is given for three different values of the temperature (100, 200, 300 °C) for five different values of the $\mathrm{GHSV_{RT}}$ (5000, 10000, 15000, 20000, 30000 $\mathrm{h^{-1}}$) based on room temperature ($T_{\mathrm{ref}} = 20°\,\mathrm{C}$). The NH_3/NO feed ratio is 1. In [39], the effectiveness factor is only given for $\mathrm{GHSV_{RT}} = 10000\,\mathrm{h^{-1}}$; it decreases from 0.867 to 0.456 when the temperature increases from 100 °C to 300 °C. Here, this temperature dependence is fitted as $\eta(T) = 2.866 \cdot \exp(-0.003213 \cdot T/\mathrm{K})$ and adopted for all values of the GHSV. The size of the square channels ($w = 1.4\,\mathrm{mm}$) corresponds by the theory of shape normalization to $a = 0.7\,\mathrm{mm}$. The paper [39] does not explicitly state the monolith length though is enters in their conversion model. In the present model, it is only the ratio U/L that enters into the normalized transversal diffusion time scale

which can be computed from $\mathrm{GHSV}_{\mathrm{ref}}$ using Eq. (55). For α, taking Eq. (52) into account, we obtain the proportionality $\alpha \propto \mathrm{GHSV}_{\mathrm{RT}} \cdot T^{-0.75}$ from Eq. (55). This dependence is reflected by the dashed curves in Fig. 8, which decrease with T and increase with $\mathrm{GHSV}_{\mathrm{RT}}$. We remark that an increase of α shifts the process to mass transfer limited operation. However, since all α values in Fig. 8 are much lower than 1 this should not be an issue here.

For computing the Damköhler number as function of temperature by Eq. (53), the pre-exponential factor A_{NO} and the activation energy E_{NO} are required. Both kinetic parameters are estimated from the experimental data [39] by the procedure outlined in Sect. 3.7. To this end, for each temperature and $\mathrm{GHSV}_{\mathrm{RT}}$ the value of $k_{\mathrm{w,int}}$ is computed using Eq. (48) in combination with $Da_{\mathrm{w}}(\omega_5)$ given in Eq. (B.9) of the Supplemental Material. The data obtained in this way are represented by symbols in Fig. 9, showing a plot of $\ln(k_{\mathrm{w,int}})$ versus the inverse absolute temperature. All symbols fall almost on one straight line which indicates the validity of the Arrhenius law. A linear least-squares fit over all data yields $A_{\mathrm{NO}} = 23.52\,\mathrm{m/s}$ (intercept) and $E_{\mathrm{NO}} = 30.88\,\mathrm{kJ/mol}$ (slope), while a fit where the supposed outlier at 300 °C and $\mathrm{GHSV}_{\mathrm{RT}} = 5000\,\mathrm{h}^{-1}$ is excluded gives $A_{\mathrm{NO}} = 33.1\,\mathrm{m/s}$ and $E_{\mathrm{NO}} = 32.01\,\mathrm{kJ/mol}$. The latter values are somewhat larger than those given by Bai & Chu [48] for the 3.45w% catalyst of Buzanowski & Yang [39], which are $A_{\mathrm{NO}} = 10.06\,\mathrm{m/s}$ and $E_{\mathrm{NO}} = 26.63\,\mathrm{kJ/mol}$. It should be noted that in the case when $\eta = 1$ is assumed so that $k_{\mathrm{w,int}} = k_{\mathrm{w,obs}}$, the data do not fall on a straight line and thus cannot be fitted by the Arrhenius law over the entire temperature range (see Fig. SM-5 in Supplemental Material). This indicates, that the present method for estimating $k_{\mathrm{w,int}}$ from experimental conversion data can be used to identify if mass transfer limitations in the washcoat may exist or not.

Figure 8 displays the temperature dependence of the Damköhler number computed by Eq. (53) for the two sets of kinetic parameters. From 100 °C to 300 °C (the measurement range in [39]), the Damköhler number with kinetic data from BC increases from about 0.04 to 0.4, while the curve with present fitted kinetic data result in somewhat lower values. With values of α and Da_{w} both below 0.4, the operating conditions correspond to the lower left quarter of the 3D conversion plot in Fig. 7, and are well within the valid range of the present conversion model X_5 (cf. Figure 6 and criterion in Eq. (46)).

Figure 10 compares the predictions by the present model X_5 (lines) with the measured conversion (open symbols) and model predictions (×) from Buzanowski & Yang [39]. To illustrate the effect of the uncertainty of kinetic parameters on the light-off curve, results of the present model are shown for $A_{\mathrm{NO}} = 23.52\,\mathrm{m/s}$ and $E_{\mathrm{NO}} = 30.88\,\mathrm{kJ/mol}$ (solid lines) and for $A_{\mathrm{NO}} = 33.1\,\mathrm{m/s}$ and $E_{\mathrm{NO}} = 32.01\,\mathrm{kJ/mol}$ (dashed lines). The light-off curves of the present model show the characteristic sigmoidal shape. The light-off temperature, which is defined by the temperature at which the conversion is 0.5, shifts with increase of $\mathrm{GHSV}_{\mathrm{RT}}$ to

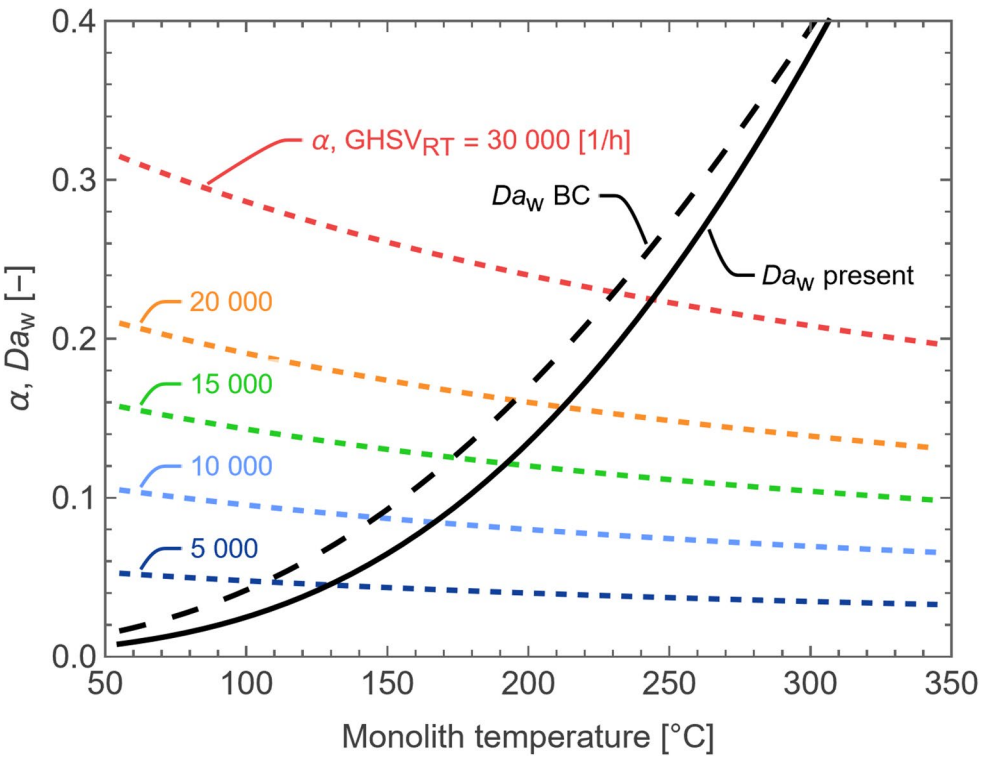

Fig. 8 Normalized transversal diffusion time scale α for different values of the $\mathrm{GHSV}_{\mathrm{RT}}$ (colored short-dashed lines) and Damköhler number Da_{w} (black solid and black long-dashed lines) versus temperature for experimental conditions of Buzanowski & Yang [39]. The Damköhler numbers are computed with $A_{\mathrm{NO}} = 10.06\,\mathrm{m/s}$ and $E_{\mathrm{NO}} = 26.63\,\mathrm{kJ/mol}$ (BC [48]) and $A_{\mathrm{NO}} = 23.52\,\mathrm{m/s}$ and $E_{\mathrm{NO}} = 30.88\,\mathrm{kJ/mol}$ (present), respectively

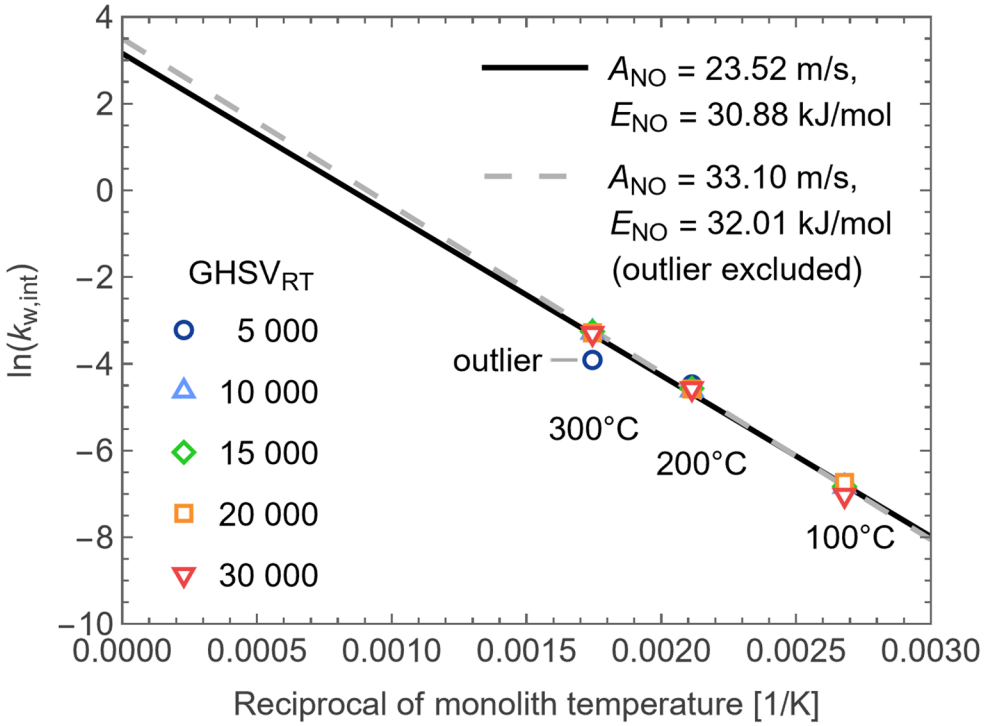

Fig. 9 Logarithm of intrinsic rate constant (symbols) estimated from experimental data of Buzanowski & Yang [39] versus reciprocal monolith temperature. Solid line: linear least-square fit to all data; dashed line: similar but with indicated outlier excluded

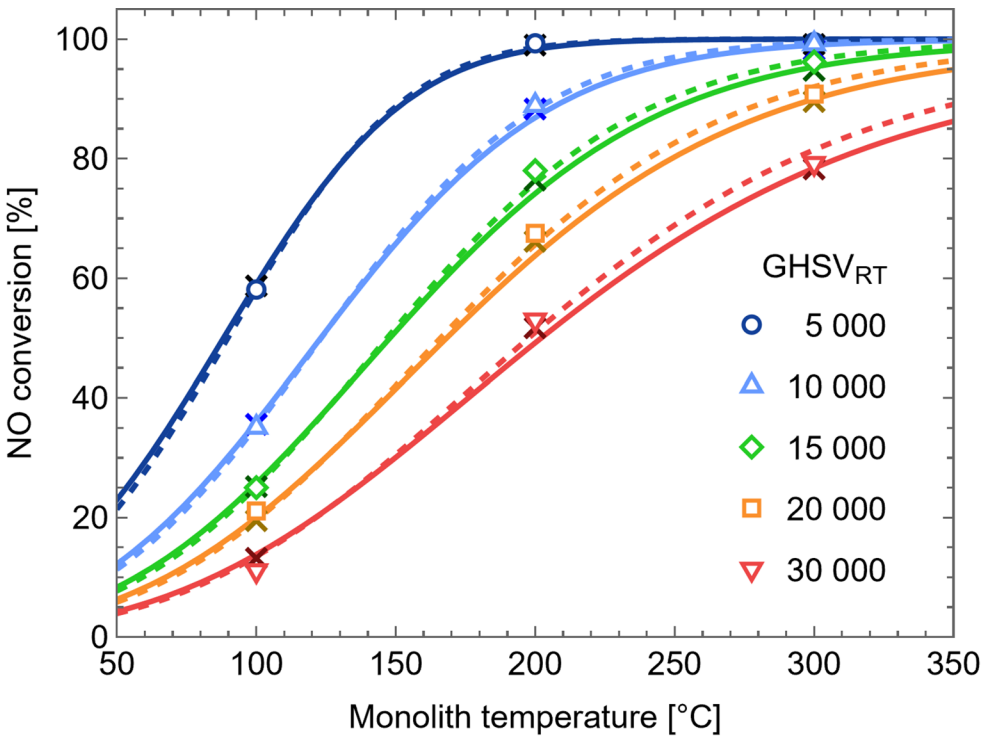

Fig. 10 NO conversion as function of temperature for five different values of the GHSV$_{RT}$. Comparison of present model X_5 (lines) with experimental data (open symbols) and model predictions (×) from Buzanowski & Yang [39], Table III. Solid lines correspond to kinetic parameters A_{NO}=23.52 m/s, and E_{NO}=32.01 kJ/mol obtained by a fit with the outlier excluded

higher temperature. This can be attributed to the increase of α with GHSV$_{RT}$ (Fig. 8) which goes along with reduced conversion (Fig. 7). The agreement of the present model with the experimental conversion data − across the entire temperature range and for all GHSV$_{RT}$ values − can be classified as good to satisfactory. For the two lowest values of GHSV$_{RT}$, the differences in conversion predicted by the present model with the two sets of kinetic parameters is very small. However, the differences increase with the increase of GHSV$_{RT}$. The reason for this could be that the effectiveness factor is a function not only of temperature, but also of GHSV$_{RT}$. While for $T = 200°$ C the set with larger values of A_{NO} and E_{NO} gives a better agreement with the measurements, the opposite is true for

$T = 300°$ C. Overall, a reasonably good agreement over wide ranges of temperature and $\mathrm{GHSV_{RT}}$ is obtained with fixed kinetic parameters; this highlights the reliability and predictive capabilities of the proposed model.

4.2.2 Beeckman and Hegedus

Beeckman & Hegedus (BH) [89] performed experiments with a monolith of length $L = 15$ cm, open frontal area $\mathrm{OFA} = 0.6$ and square channels of cell size $w = 6$ mm. Applying shape normalization once again, we choose for a half the side-length of the square channel, such that $a = w/2 = 3$ mm. The authors considered two different catalysts. In this paper, conversion data for $\mathrm{GHSV_{STP}} = 8600\,\mathrm{h}^{-1}$ at standard temperature and pressure ($T_{\mathrm{ref}} = 0°$ C, 1 atm) for catalyst A are used for comparison. Figure 11 shows the corresponding normalized transversal diffusion time scale computed from Eq. (55) as function of temperature. An increase of T from 200 °C to 500 °C goes along with a decrease of α from 1.3 to 0.9. Over this temperature range, the mean velocity U increases from about 1 m/s to 1.7 m/s, while the kinematic viscosity of nitrogen increases from $3.4 \cdot 10^{-5}\,\mathrm{m^2/s}$ to $7.8 \cdot 10^{-5}\,\mathrm{m^2/s}$. Accordingly, the Reynolds number is estimated to decrease from 184 to 130.

To compute the Damköhler number, we need data for A_{NO} and E_{NO}. Beeckman & Hegedus [89] proposed a 1D lumped parameter model for the SCR process. They used a mass transfer coefficient to represent the flow characteristics and the chemical kinetics in the SCR system. Their model accounted for external diffusion in the gas phase and intrapore diffusional phenomena. The authors determined kinetic parameters by fitting their model to measured data and obtained for the pre-exponential factor $A_{\mathrm{NO}} = 86.4\,\mathrm{m/s}$ and for the activation energy $E_{\mathrm{NO}} = 79.5\,\mathrm{kJ/mol}$. Later, Bai & Chwu (BC) [48, Table 2], determined by comparison of numerical results obtained by 2D finite difference solution of the governing equations in a square channel the values $A_{\mathrm{NO}} = 35.2\,\mathrm{m/s}$ and $E_{\mathrm{NO}} = 33.4\,\mathrm{kJ/mol}$ for the catalyst A of BH [89]. Applying the procedure outlined in Sect. 3.7 for the data of BH yields Fig. 12; as can be seen, the three data point for $k_{\mathrm{w,obs}}$ can well be fitted by a straight line. This suggests that one may assume $\eta = 1$ for this experiment so that $k_{\mathrm{w,int}} = k_{\mathrm{w,obs}}$. In this way, we obtain $A_{\mathrm{NO}} = 83.3\,\mathrm{m/s}$ and $E_{\mathrm{NO}} = 39.04\,\mathrm{kJ/mol}$ for this catalyst. The curves for Da_{w} resulting from the latter values and those of BC are shown in Fig. 11. The kinetic data of BH give unreasonably low values for Da_{w} below 0.01 and are disregarded. For the kinetic data of BC, the Damköhler increases over the temperature range 200–500 °C from about 0.45 to 5.2, and for the present fit from 0.26 to 5.2. The values of α and Da_{w} in Fig. 11 can be related to the 3D conversion plot over both parameters in Fig. 7. Accordingly, the experimental conditions [89] correspond to $\alpha \approx 1$ where conversion depends strongly on Da_{w}. With $\alpha \approx 1$ and $Da_{\mathrm{w}} \approx 4$ at $T = 400°$ C, the operation of the catalytic monolith is likely to be close to the mass transfer limited regime which is not surprising given the large cell size.

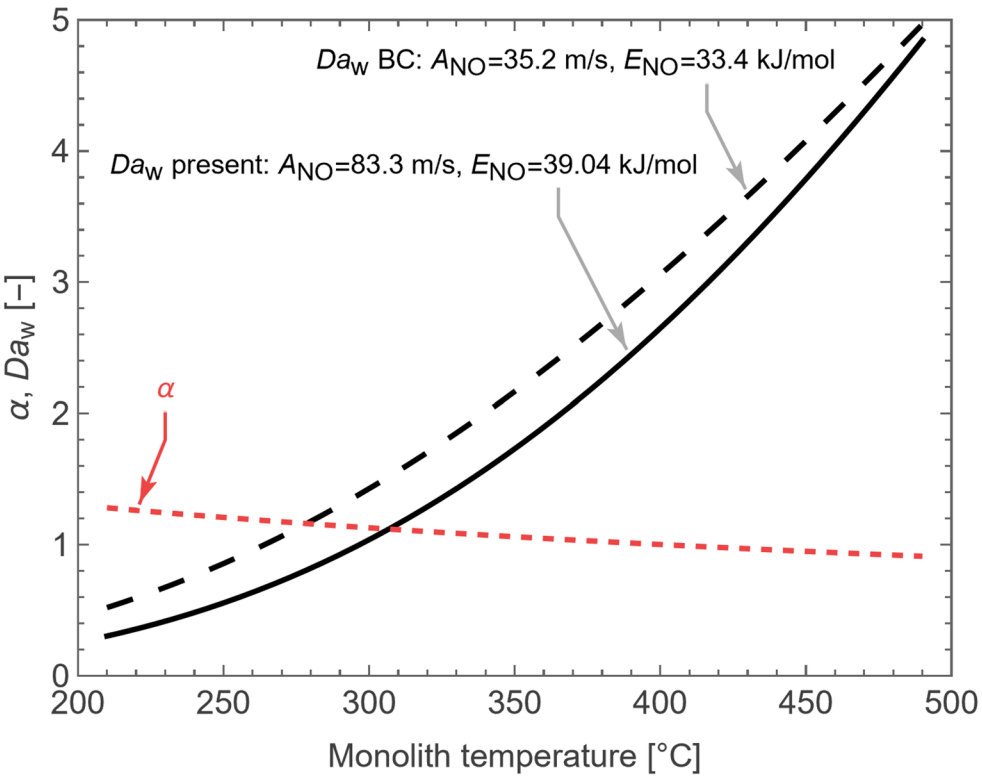

Fig. 11 Normalized transversal diffusion time scale α (red dashed line) and heterogenous Damköhler number Da_{w} (black lines) versus temperature for experimental conditions of Beeckman & Hegedus [89] at $\mathrm{GHSV_{STP}} = 8600\,\mathrm{h}^{-1}$. Curves for Da_{w} correspond to kinetic parameters of Bai & Chwu [48] (long-dashed) and present fit (solid)

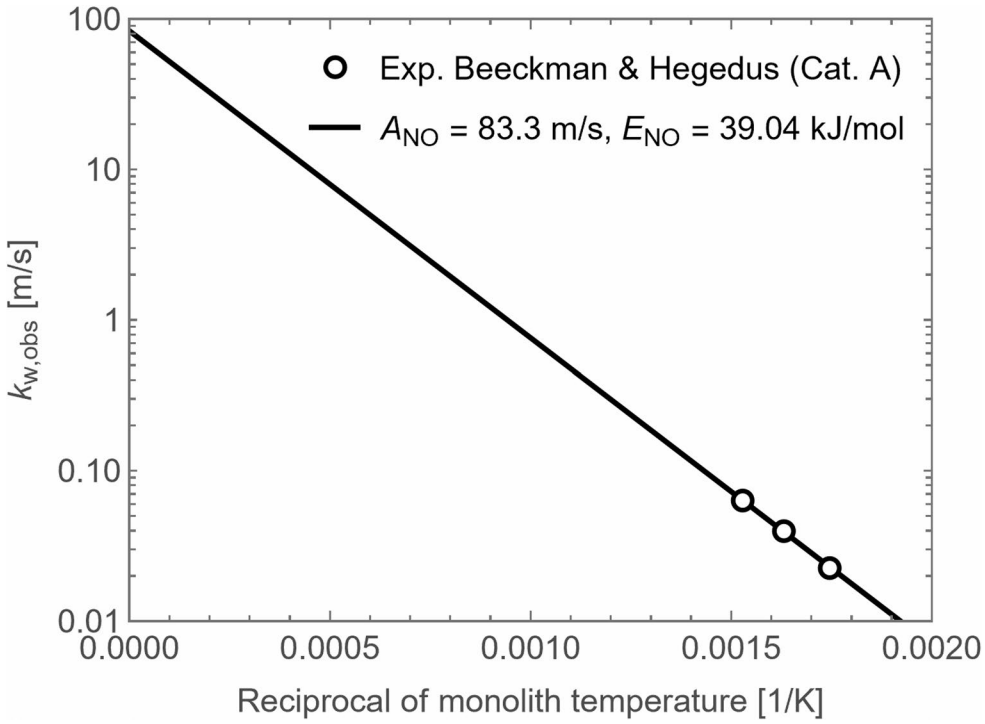

Fig. 12 Rate constant (symbols) estimated from experimental data [48] versus reciprocal monolith temperature. Solid line: linear fit

Figure 13 compares the measured NO conversion [89] with the present conversion model X_5 for two sets of kinetic parameters. The set of BC overestimates the experimental conversion, with the overestimation decreasing as the temperature increases. Good agreement with the experimental conversion is achieved using the kinetic parameters determined through the present fitting procedure; however, given the narrow conversion range of 70–85%, this is of limited significance.

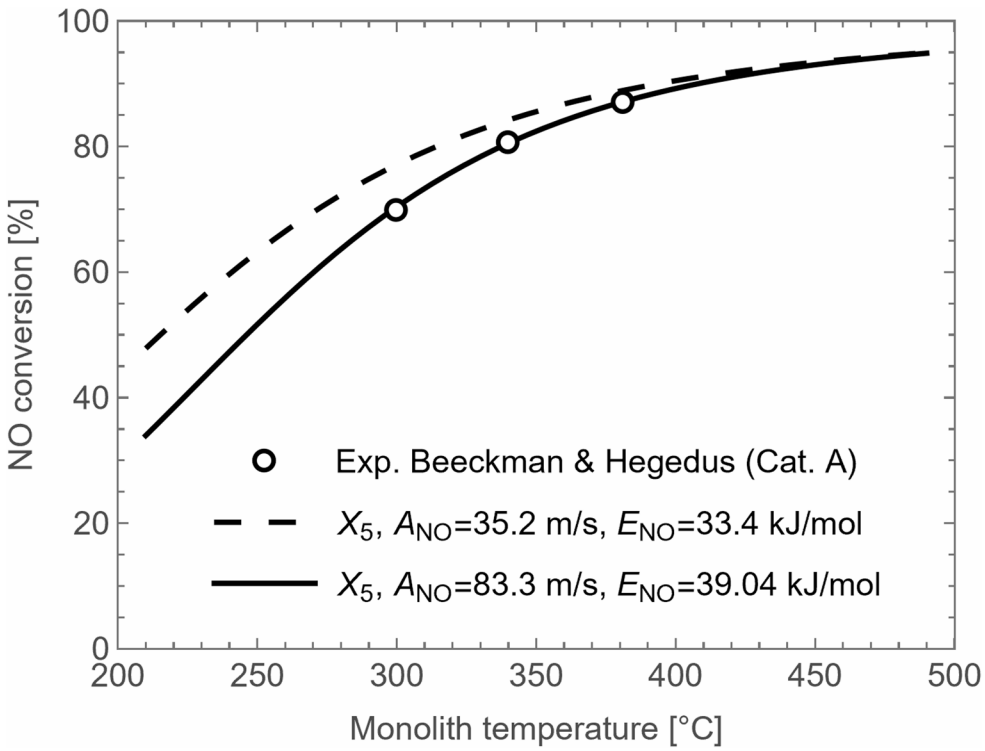

Fig. 13 NO conversion as function of temperature. Symbols represent experimental data [89] and lines present model X_5, Long-dashed line: kinetic data from Bai & Chwu [48], solid line: present kinetic data determined from Fig. 12

5 Conclusions

In this paper, the classical problem of convective-diffusion with reaction in laminar (Poiseuille) flow through a circular tube is revisited. The analysis is restricted to the steady-state, isothermal case involving irreversible first-order reactions in the gas-phase and at the wall, with negligible axial diffusion. From the normalized reactant mass balance equation, a novel approximate solution for the local concentration field in form of an infinite series is derived which automatically fulfills the boundary condition at the catalytic wall but violates the condition of uniform inlet concentration. Flow-weighted integration of the truncated series yields a novel one-term exponential model for exit concentration and overall conversion in terms of three non-dimensional groups: the normalized transversal diffusion time scale (α), and the Damköhler numbers of the heterogeneous ($Da_{\mathrm{w}} > 0$) and homogeneous ($Da_{\mathrm{b}} \geq 0$) reactions. The computational effort of the model is minimal, as only the root of a polynomial of the Damköhler numbers needs to be determined. The accuracy of the model is tested against the numerical solution of the PDE for the case of a heterogeneous reaction ($Da_{\mathrm{b}} = 0$), and the validity of the model is found to be restricted to the Graetz regime with fully developed concentration field corresponding to $\alpha \leq 1$.

In conjunction with the Arrhenius law and the relationships describing the temperature dependence of the diffusion coefficient and the effectiveness factor, the proposed model enables the determination of observed/intrinsic rate constants from experimental conversion data − as demonstrated by the example of the heterogeneous selective catalytic reduction of NO. The model also enables the instant assessment of the sensitivity of the light-off curve of a monolith reactor to parameter variations, e.g., by use of Mathematica program (see Wolfram CDF file in Supplemental Material). As thus, it provides a platform for a fundamental understanding of the interaction between structural parameters of the monolith (cell size, OFA) with operational parameters (GHSV) and kinetic parameters (pre-exponential factor, activation energy) under varying temperature. The model may therefore be useful to support the design of monolith converters or kinetic optimization studies. It should be mentioned, however, that in reality, the first-order reaction law used here and other simplifying assumptions such as isothermal conditions only occur in limited cases.

Supplementary Information The online version contains supplementary material available at https://doi.org/10.1007/s40825-026-00307-9.

Acknowledgements The author thanks members of the Deutschmann group at KIT for scientific discussions (Matthias Hettel, Steffen Tischer) and for IT support concerning Mathematica software (Martin Spoo).

Author contributions This manuscript has only one author.

Funding Open Access funding enabled and organized by Projekt DEAL. No funding was received for conducting this study.

Data Availability No datasets were generated or analysed during the current study.

Declarations

Competing interests The author declares no competing interests.

Open Access This article is licensed under a Creative Commons Attribution 4.0 International License, which permits use, sharing, adaptation, distribution and reproduction in any medium or format, as long as you give appropriate credit to the original author(s) and the source, provide a link to the Creative Commons licence, and indicate if changes were made. The images or other third party material in this article are included in the article's Creative Commons licence, unless indicated otherwise in a credit line to the material. If material is not included in the article's Creative Commons licence and your intended use is not permitted by statutory regulation or exceeds the permitted use, you will need to obtain permission directly from the copyright holder. To view a copy of this licence, visit http://creativecommons.org/licenses/by/4.0/.

References

1. Lott, P., Deutschmann, O.: Heterogeneous chemical reactions - A cornerstone in emission reduction of local pollutants and greenhouse gases. Proc. Combust. Inst. **39**(3), 3183–3215 (2023). https://doi.org/10.1016/j.proci.2022.06.001
2. Votsmeier, M., Kreuzer, T., Gieshoff, J., Lepperhoff, G., Elvers, B.: Automobile Exhaust Control. In: Ullmann's Encyclopedia of Industrial Chemistry. pp 1–19. (2019). https://doi.org/10.1002/14356007.a03_189.pub3
3. Woo, M., Gu, Y., Kim, G.-M., Kim, M., Kim, H.S., Lim, D.-H.: Numerical Study on NO Conversion Characteristics of Ceramic and Metallic Monoliths Under Steady-State External Heat Loss in Marine After-Treatment System. Korean J. Chem. Eng. **41**(1), 225–235 (2024). https://doi.org/10.1007/s11814-024-00075-8
4. Heck, R.M., Farrauto, R.J., Gulati, S.T.: Catalytic air pollution control: commercial technology, Third edn Wiley-Interscience, New York (2009)
5. Ablow, C.M., Wise, H.: Theoretical-Analysis of Catalytic Combustion in a Monolith Reactor. Combust. Sci. Technol. **21**(1–2), 35–42 (1979). https://doi.org/10.1080/00102207908946916
6. Schwiedernoch, R., Tischer, S., Correa, C., Deutschmann, O.: Experimental and numerical study on the transient behavior of partial oxidation of methane in a catalytic monolith. Chem. Eng. Sci. **58**(3), 633–642 (2003). https://doi.org/10.1016/S0009-2509(02)00589-4
7. Williams, J.L.: Monolith structures, materials, properties and uses. Catal. Today. **69**(1), 3–9 (2001). https://doi.org/10.1016/S0920-5861(01)00348-0
8. Hayes, R.E., Kolaczkowski, S.T.: Mass and Heat-Transfer Effects in Catalytic Monolith Reactors. Chem. Eng. Sci. **49**(21), 3587–3599 (1994). https://doi.org/10.1016/0009-2509(94)00164-2
9. Groppi, G., Belloli, A., Tronconi, E., Forzatti, P.: Analysis of Multidimensional Models of Monolith Catalysts for Hybrid Combustors. AIChE J. **41**(10), 2250–2260 (1995). https://doi.org/10.1002/aic.690411008
10. Leclerc, J.-P., Schweich, D.: Modeling Catalytic Monoliths for Automobile Emission Control. In: de Lasa, H.I., Doğu, G., Ravella, A. (eds.) Chemical Reactor Technology for Environmentally

Safe Reactors and Products, pp. 547–576. Springer Netherlands, Dordrecht (1993). https://doi.org/10.1007/978-94-011-2747-9_23
11. Hayes, R.E., Cornejo, I.: Multi-scale modelling of monolith reactors: A 30-year perspective from 1990 to 2020. Can. J. Chem. Eng. **99**(12), 2589–2606 (2021). https://doi.org/10.1002/cjce.24144
12. Siemund, S., Leclerc, J.-P., Schweich, D., Prigent, M., Castagna, F.: Three-way monolithic converter: Simulations versus experiments. Chem. Eng. Sci. **51**(15), 3709–3720 (1996). https://doi.org/10.1016/0009-2509(96)00018-8
13. Cornejo, I., Hayes, R.E.: A Review of the Critical Aspects in the Multi-Scale Modelling of Structured Catalytic Reactors. Catalysts **11**(1), 89 (2021). https://doi.org/10.3390/catal11010089
14. Nagarajan, P.C., Ström, H., Sjöblom, J.: Methodology for Reduced-Order Multichannel Modeling of a Catalytic Converter. Ind. Eng. Chem. Res. **63**(41), 17462–17476 (2024). https://doi.org/10.1021/acs.iecr.4c01571
15. Hettel, M., Daymo, E., Schmidt, T., Deutschmann, O.: CFD-Modeling of fluid domains with embedded monoliths with emphasis on automotive converters. Chem. Eng. Process. **147**, 107728 (2020). https://doi.org/10.1016/j.cep.2019.107728
16. Hettel, M., Diehm, C., Bonart, H., Deutschmann, O.: Numerical simulation of a structured catalytic methane reformer by DUO: The new computational interface for OpenFOAM® and DETCHEM™. Catal. Today. **258**, 230–240 (2015). https://doi.org/10.1016/j.cattod.2015.02.011
17. Raja, L.L., Kee, R.J., Deutschmann, O., Warnatz, J., Schmidt, L.D.: A critical evaluation of Navier–Stokes, boundary-layer, and plug-flow models of the flow and chemistry in a catalytic-combustion monolith. Catal. Today. **59**(1), 47–60 (2000). https://doi.org/10.1016/S0920-5861(00)00271-6
18. Mladenov, N., Koop, J., Tischer, S., Deutschmann, O.: Modeling of transport and chemistry in channel flows of automotive catalytic converters. Chem. Eng. Sci. **65**(2), 812–826 (2010). https://doi.org/10.1016/j.ces.2009.09.034
19. Lie, A.B.K., Hoebink, J., Marin, G.B.: The Effects of Oscillatory Feeding of CO and O_2 on the Performance of a Monolithic Catalytic-Converter of Automobile Exhaust-Gas - a Modeling Study. Chem. Eng. J. **53**(1), 47–54 (1993). https://doi.org/10.1016/0923-0467(93)80006-I
20. Roduit, B., Baiker, A., Bettoni, F., Baldyga, J., Wokaun, A.: 3-D modeling of SCR of NO_x by NH_3 on vanadia honeycomb catalysts. AIChE J. **44**(12), 2731–2744 (1998). https://doi.org/10.1002/aic.690441214
21. Tischer, S., Deutschmann, O.: Recent advances in numerical modeling of catalytic monolith reactors. Catal. Today. **105**(3–4), 407–413 (2005). https://doi.org/10.1016/j.cattod.2005.06.061
22. Nagarajan, P.C., Ström, H., Sjöblom, J.: Transient Flow Uniformity Evolution in Realistic Exhaust Gas Aftertreatment Systems Using 3D-CFD. Emission Contr Sci. Technol. **8**(3), 154–170 (2022). https://doi.org/10.1007/s40825-022-00217-6
23. Tronconi, E., Forzatti, P.: Adequacy of Lumped Parameter Models for SCR Reactors with Monolith Structure. AIChE J. **38**(2), 201–210 (1992). https://doi.org/10.1002/aic.690380205
24. Depcik, C., Assanis, D.: One-dimensional automotive catalyst modeling. Prog Energy Combust. Sci. **31**(4), 308–369 (2005). https://doi.org/10.1016/j.pecs.2005.08.001
25. Hayes, R.E., Kolaczkowski, S.T.: A study of Nusselt and Sherwood numbers in a monolith reactor. Catal. Today. **47**(1), 295–303 (1999). https://doi.org/10.1016/S0920-5861(98)00310-1
26. Gupta, N., Balakotaiah, V.: Heat and mass transfer coefficients in catalytic monoliths. Chem. Eng. Sci. **56**(16), 4771–4786 (2001). https://doi.org/10.1016/S0009-2509(01)00134-8
27. Holmgren, A., Andersson, B.: Mass transfer in monolith catalysts - CO oxidation experiments and simulations. Chem. Eng. Sci. **53**(13), 2285–2298 (1998). https://doi.org/10.1016/S0009-2509(98)00080-3
28. Santos, A., Bahamonde, A., Schmid, M., Avila, P., García-Ochoa, F.: Mass transfer influences on the design of selective catalytic reduction (SCR) monolithic reactors. Chem. Eng. Process. Process. Intensif. **37**(2), 117–124 (1998). https://doi.org/10.1016/S0255-2701(97)00057-3
29. Bensalem, O., Ernst, W.R.: Mathematical-Modeling of Homogeneous-Heterogeneous Reactions in Monolithic Catalysts. Combust. Sci. Technol. **29**(1–2), 1–13 (1982). https://doi.org/10.1080/00102208208923583
30. Ratnakar, R.R., Dadi, R.K., Balakotaiah, V.: Multi-scale reduced order models for transient simulation of multi-layered monolith reactors. Chem. Eng. J. **352**, 293–305 (2018). https://doi.org/10.1016/j.cej.2018.04.053
31. Tu, M., Ratnakar, R.R., Balakotaiah, V.: Reduced order models with local property dependent transfer coefficients for real time simulations of monolith reactors. Chem. Eng. J. **383**, 123074 (2020). https://doi.org/10.1016/j.cej.2019.123074
32. Tu, M., Balakotaiah, V.: Low-dimensional models for real time simulations of monolith reactors with dual washcoat layers. Chem. Eng. J. **429**, 132153 (2022). https://doi.org/10.1016/j.cej.2021.132153
33. Konstandopoulos, A.G., Johnson, J.H.: Wall-Flow Diesel Particulate Filters—Their Pressure Drop and Collection Efficiency. Paper presented at the SAE International Congress and Exposition, Detroit, Michigan, United States, February 27, 1989 (1989)
34. Watling, T.C.: Simulating Catalytic Reaction and Soot Oxidation in Coated Particulate Filters: a Simplified Modelling Framework Including Diffusion Effects. Emission Contr Sci. Technol. **9**(2), 93–119 (2023). https://doi.org/10.1007/s40825-023-00226-z
35. Watling, T.C.: Simplified Analytic Particulate Filter Backpressure Models Revisited: Derivation of the Additive Flow Resistance Model. Emission Contr Sci. Technol. **11**(1), 8 (2025). https://doi.org/10.1007/s40825-025-00259-6
36. Solomon, R.L., Hudson, J.L.: Heterogeneous and Homogeneous Reactions in a Tubular Reactor. AIChE J. **13**(3), 545–550 (1967). https://doi.org/10.1002/aic.690130326
37. Higuera, F.J., de la Mora, J.F.: The reactive Graetz problem for a first order homogeneous decomposition reaction, and the limit of moderately large reaction constants. Phys. Fluids. **35**(9), 093616 (2023). https://doi.org/10.1063/5.0168890
38. Mansour, A.R., Sheboul, M., Hussein, A.M., Nusayr, A.: An analytical solution for diffusion and reaction in a laminar flow tubular reactor. Int. Commun. Heat Mass Transfer. **16**(4), 603–608 (1989). https://doi.org/10.1016/0735-1933(89)90063-8
39. Buzanowski, M.A., Yang, R.T.: Simple Design of Monolith Reactor for Selective Catalytic Reduction of NO for Power-Plant Emission Control. Ind. Eng. Chem. Res. **29**(10), 2074–2078 (1990). https://doi.org/10.1021/ie00106a015
40. Lopes, J.P., Rodrigues, A.E., Cardoso, S.S.S.: Approximate Calculation of Conversion with Kinetic Normalization for Finite Reaction Rates in Wall-Coated Microchannels. AIChE J. **57**(10), 2870–2887 (2011). https://doi.org/10.1002/aic.12483
41. Lopes, J.P., Cardoso, S.S.S., Rodrigues, A.E.: Interplay between channel and catalyst operating regimes in wall-coated microreactors. Chem. Eng. J. **227**, 42–55 (2013). https://doi.org/10.1016/j.cej.2012.11.056
42. Lee, S.-T., Aris, R.: On the Effects of Radiative Heat-Transfer in Monoliths. Chem. Eng. Sci. **32**(8), 827–837 (1977). https://doi.org/10.1016/0009-2509(77)80068-7
43. Balakotaiah, V., West, D.H.: Shape normalization and analysis of the mass transfer controlled regime in catalytic monoliths. Chem. Eng. Sci. **57**(8), 1269–1286 (2002). https://doi.org/10.1016/S0009-2509(02)00059-3
44. Bhattacharya, M., Harold, M.P., Balakotaiah, V.: Shape normalization for catalytic monoliths. Chem. Eng. Sci. **59**(18), 3737–3766 (2004). https://doi.org/10.1016/j.ces.2004.02.020

45. Hegedus, L.L.: Temperature Excursions in Catalytic Monoliths. AIChE J. **21**(5), 849–853 (1975). https://doi.org/10.1002/aic.690210503
46. Wu, J., Platzer, B.: Systematic analysis of the effect of temperature profiles on reactions in tubular reactors. Z. Angew Math. Mech. **91**(4), 300–329 (2011). https://doi.org/10.1002/zamm.201000015
47. Heinisch, R., Rogowski, A., Schütt, E.: Modell eines isothermen Wabenreaktors. Wärme und Stoffübertragung. **27**(3), 177–183 (1992). https://doi.org/10.1007/Bf01599932
48. Bai, H., Chwu, J.-W.: Theoretical analysis of selective catalytic reduction catalysts. J. Environ. Eng. **123**(5), 431–436 (1997). https://doi.org/10.1061/(Asce)0733-9372(1997)123:5(431)
49. Bai, H., Chwu, J.-W.: Design Model for Selective Catalytic Reduction Process: Solution of Convective Diffusion and NO_x Reaction. J. Environ. Eng. **124**(12), 1220–1226 (1998). (1998)124:12(1220) https://doi.org/10.1061/(ASCE)0733-9372
50. Steiner, T., Neurauter, D., Moewius, P., Pfeifer, C., Schallhart, V., Moeltner, L.: Heat-Up Performance of Catalyst Carriers - A Parameter Study and Thermodynamic Analysis. Energies. **14**(4), 964 (2021). https://doi.org/10.3390/en14040964
51. Young, L.C., Finlayson, B.A.: Mathematical-Models of Monolith Catalytic-Converter.2. Application to Automobile Exhaust. AIChE J. **22**(2), 343–353 (1976). https://doi.org/10.1002/aic.690220217
52. Young, L.C., Finlayson, B.A.: Mathematical-Models of Monolith Catalytic-Converter.1. Development of Model and Application of Orthogonal Collocation. AIChE J. **22**(2), 331–343 (1976). https://doi.org/10.1002/aic.690220216
53. Katz, S.: Chemical reactions catalysed on a tube wall. Chem. Eng. Sci. **10**(4), 202–211 (1959). https://doi.org/10.1016/0009-2509(59)80054-3
54. Dang, V.-D., Steinberg, M.: Convective Diffusion with Homogeneous and Heterogeneous Reactions in a Tube. J. Phys. Chem. **84**(2), 214–219 (1980). https://doi.org/10.1021/j100439a018
55. Lauwerier, H.A.: A diffusion problem with chemical reaction. Appl. Sci. Res. Sect. A. **8**(1), 366–376 (1959). https://doi.org/10.1007/BF00411762
56. Wissler, E.H., Schechter, R.S.: A further note on a diffusion problem with chemical reaction. Appl. Sci. Res. **10**(1), 198–204 (1961). https://doi.org/10.1007/BF00411913
57. Subramanian, R.S., Gill, W.N., Marra, R.A.: Dispersion Models of Unsteady Tubular Reactors. Can. J. Chem. Eng. **52**(5), 563–568 (1974). https://doi.org/10.1002/cjce.5450520504
58. Homsy, R.V., Strohman, R.D.: Diffusion and Chemical Reaction in a Tubular Reactor with Non-Newtonian Laminar Flow. AIChE J. **17**(1), 215–219 (1971). https://doi.org/10.1002/aic.690170142
59. Lawal, A.: Convective diffusion of power-law fluids inside ducts with single homogeneous and catalytic wall reactions. Chem. Eng. J. **62**(1), 51–60 (1996). https://doi.org/10.1016/0923-0467(95)03053-0
60. Brauer, H., Schlüter, H.: Konvektiver Stoffaustausch mit heterogener chemischer Reaktion. Chem. Ing. Tech. **37**(11), 1107–1117 (1965). https://doi.org/10.1002/cite.330371106
61. Hsu, C.-J.: A Method of Solution for Mass Transfer with Chemical Reaction under Conditions of Viscous Flow in a Tubular Reactor. AIChE J. **11**(5), 938–940 (1965). https://doi.org/10.1002/aic.690110536
62. Dang, V.-D., Steinberg, M.: Laminar flow mass transfer with axial diffusion in a tube with chemical reactions. Chem. Eng. Sci. **32**(3), 326–328 (1977). https://doi.org/10.1016/0009-2509(77)80212-1
63. Chakraborty, S., Balakotaiah, V.: Low-dimensional models for describing mixing effects in laminar flow tubular reactors. Chem. Eng. Sci. **57**(13), 2545–2564 (2002). https://doi.org/10.1016/S0009-2509(02)00129-X
64. Balakotaiah, V., Chakraborty, S.: Averaging theory and low-dimensional models for chemical reactors and reacting flows. Chem. Eng. Sci. **58**(21), 4769–4786 (2003). https://doi.org/10.1016/j.ces.2002.11.002
65. Berger, R.J., Kapteijn, F.: Coated-wall reactor modeling-criteria for neglecting radial concentration gradients. 1. Empty reactor tubes. Ind. Eng. Chem. Res. **46**(12), 3863–3870 (2007). https://doi.org/10.1021/ie0612313
66. Lopes, J.P., Cardoso, S.S.S., Rodrigues, A.E.: Criteria for kinetic and mass transfer control in a microchannel reactor with an isothermal first-order wall reaction. Chem. Eng. J. **176**, 3–13 (2011). https://doi.org/10.1016/j.cej.2011.05.088
67. Morini, G.L.: Scaling effects for liquid flows in microchannels. Heat Transfer Eng. **27**(4), 64–73 (2006). https://doi.org/10.1080/01457630500523865
68. Wörner, M.: Dispersion and residence time distribution of laminar tubular flow in the transition regime – models for flow chemistry and beyond. Chem. Eng. Sci. **318**, 122116 (2025). https://doi.org/10.1016/j.ces.2025.122116
69. Judeikis, H.S., Stewart, T.B.: Laboratory Measurement of SO_2 Deposition Velocities on Selected Building-Materials and Soils. Atmos. Environ. **10**(9), 769–776 (1976). https://doi.org/10.1016/0004-6981(76)90078-0
70. Graetz, L.: Ueber die Wärmeleitungsfähigkeit von Flüssigkeiten. 1. Abhandlung. Ann. Phys. **254**(1), 79–94 (1883). https://doi.org/10.1002/andp.18822540106
71. Damköhler, G.: Einfluss von Diffusion, Strömung und Wärmetransport auf die Ausbeute bei chemisch-technischen Reaktionen. In: Eucken, A., Jakob, M. (eds.) Der Chemie-Ingenieur, Bd. III, Teil 1, vol. vol III, Teil 1, pp. 359–485. Akademische Verlagsgesellschaft, Leipzig (1937)
72. Lopes, J.P., Cardoso, S.S.S., Rodrigues, A.E.: Bridging the gap between Graetz's and Lévêque's analyses for mass/heat transfer in a channel with uniform concentration or flux at the wall. AIChE J. **58**(6), 1880–1892 (2012). https://doi.org/10.1002/aic.12719
73. Cleland, F.A., Wilhelm, R.H.: Diffusion and Reaction in Viscous-Flow Tubular Reactor. AIChE J. **2**(4), 489–497 (1956). https://doi.org/10.1002/aic.690020414
74. Rothenberg, R.I., Smith, J.M.: Heat Transfer and Reaction in Laminar Tube Flow. AIChE J. **12**(2), 213–220 (1966). https://doi.org/10.1002/aic.690120204
75. Bräuer, H.W., Fetting, F.: Stofftransport bei Wandreaktion im Einlaufgebiet eines Strömungsrohres. Chem. Ing. Tech. **38**(1), 30–35 (1966). https://doi.org/10.1002/cite.330380107
76. Walker, R.E.: Chemical Reaction and Diffusion in a Catalytic Tubular Reactor. Phys. Fluids A **4**(10), 1211–1216 (1961). https://doi.org/10.1063/1.1706198
77. Lauwerier, H.A.: The use of confluent hypergeometric functions in mathematical physics and the solution of an eigenvalue problem. Appl. Sci. Res. **2**(1), 184–204 (1951). https://doi.org/10.1007/BF00411982
78. Lauwerier, H.A.: Poiseuille Functions. Appl. Sci. Res. Section A-Mechanics Heat. Chem. Eng. Math. Methods. **3**(1), 58–72 (1951). https://doi.org/10.1007/Bf03184672
79. Ogren, P.J.: Analytical results for first-order kinetics in flow tube reactors with wall reactions. J. Phys. Chem. **79**(17), 1749–1752 (1975). https://doi.org/10.1021/j100584a001
80. Nigam, K.M., Srivastava, V.K., Nigam, K.D.P.: Homogeneous-heterogeneous reactions in a tubular reactor: An analytical solution. Chem. Eng. J. **25**(2), 147–150 (1982). https://doi.org/10.1016/0300-9467(82)80083-X
81. West, D.H., Balakotaiah, V., Jovanovic, Z.: Experimental and theoretical investigation of the mass transfer controlled regime in catalytic monoliths. Catal. Today. **88**(1–2), 3–16 (2003). https://doi.org/10.1016/j.cattod.2003.08.002

82. Gundlapally, S.R., Balakotaiah, V.: Heat and mass transfer correlations and bifurcation analysis of catalytic monoliths with developing flows. Chem. Eng. Sci. **66**(9), 1879–1892 (2011). https://doi.org/10.1016/j.ces.2011.01.045
83. Harrison, B.K., Ernst, W.R.: Catalytic Combustion in Cylindrical Channels: A Homogeneous-Heterogeneous Model. Combust. Sci. Technol. **19**(1–2), 31–38 (1978). https://doi.org/10.1080/00102207808946861
84. Cho, S.M.: Properly Apply Selective Catalytic Reduction for NO_x Removal. Chem. Eng. Prog. **90**(1), 39–45 (1994)
85. Nova, I., Tronconi, E.: Urea-SCR technology for deNOx after treatment of diesel exhausts. Fundamental and applied catalysis. Springer, New York (2014). https://doi.org/10.1007/978-1-4899-8071-7
86. Burluka, A.A., Manning, A.P.: Chemical kinetic mechanism for selective catalytic reduction of nitrogen oxides. Catal. Sci. Technol. **15**(2), 547–562 (2025). https://doi.org/10.1039/D4CY01205D
87. Duprat, F.: Light-off curve of catalytic reaction and kinetics. Chem. Eng. Sci. **57**(6), 901–911 (2002). https://doi.org/10.1016/S0009-2509(01)00409-2
88. Joshi, S.Y., Kumar, A., Luo, J., Kamasamudram, K., Currier, N.W., Yezerets, A.: New insights into the mechanism of NH_3-SCR over Cu- and Fe-zeolite catalyst: Apparent negative activation energy at high temperature and catalyst unit design consequences. Appl. Catal. B: Environ. **226**, 565–574 (2018). https://doi.org/10.1016/j.apcatb.2017.12.076
89. Beeckman, J.W., Hegedus, L.L.: Design of Monolith Catalysts for Power-Plant NO_x Emission Control. Ind. Eng. Chem. Res. **30**(5), 969–978 (1991). https://doi.org/10.1021/ie00053a020
90. Zhang, Z., Zhong, W., Pan, M., Yin, Z., Lu, K.: Multi-objective optimization of structural parameters of SCR system under Eley-Rideal reaction mechanism based on machine learning coupled with response surface methodology. Fuel Process. Technol. **265**, 108141 (2024). https://doi.org/10.1016/j.fuproc.2024.108141
91. Lefers, J.B., Lodder, P., Enoch, G.D.: Modelling of selective catalytic denox reactors – strategy for replacing deactivated catalyst elements. Chem. Eng. Technol. **14**(3), 192–200 (1991). https://doi.org/10.1002/ceat.270140307
92. Svachula, J., Ferlazzo, N., Forzatti, P., Tronconi, E., Bregani, F.: Selective Reduction of NO_x by NH_3 over Honeycomb Denoxing Catalysts. Ind. Eng. Chem. Res. **32**(6), 1053–1060 (1993). https://doi.org/10.1021/ie00018a010
93. Inomata, M., Miyamoto, A., Murakami, Y.: Mechanism of the Reaction of NO and NH_3 on Vanadium-Oxide Catalyst in the Presence of Oxygen under the Dilute Gas Condition. J. Catal. **62**(1), 140–148 (1980). https://doi.org/10.1016/0021-9517(80)90429-7
94. Marangozis, J.: Comparison and Analysis of Intrinsic Kinetics and Effectiveness Factors for the Catalytic Reduction of NO with Ammonia in the Presence of Oxygen. Ind. Eng. Chem. Res. **31**(4), 987–994 (1992). https://doi.org/10.1021/ie00004a001
95. Metkar, P.S., Harold, M.P., Balakotaiah, V.: Experimental and kinetic modeling study of NH_3-SCR of NO_x on Fe-ZSM-5, Cu-chabazite and combined Fe- and Cu-zeolite monolithic catalysts. Chem. Eng. Sci. **87**, 51–66 (2013). https://doi.org/10.1016/j.ces.2012.09.008
96. Huang, H.Y., Long, R.Q., Yang, R.T.: Kinetics of selective catalytic reduction of NO with NH_3 on Fe-ZSM-5 catalyst. Appl. Catal. A. **235**(1), 241–251 (2002). https://doi.org/10.1016/S0926-860X(02)00268-5
97. Delahay, G., Kieger, S., Tanchoux, N., Trens, P., Coq, B.: Kinetics of the selective catalytic reduction of NO by NH_3 on a Cu-faujasite catalyst. Appl. Catal. B: Environ. **52**(4), 251–257 (2004). https://doi.org/10.1016/j.apcatb.2004.04.008
98. Fuller, E.N., Schettler, P.D., Giddings, J.C.: A New Method for Prediction of Binary Gas-Phase Diffusion Coefficients. Ind. Eng. Chem. **58**(5), 19–27 (1966). https://doi.org/10.1021/ie50677a007
99. Massman, W.J.: A review of the molecular diffusivities of H_2O, CO_2, CH_4, CO, O_3, SO_2, NH_3, N_2O, NO, and NO_2 in air, O_2 and N_2 near STP. Atmos. Environ. **32**(6), 1111–1127 (1998). https://doi.org/10.1016/S1352-2310(97)00391-9

Publisher's Note Springer Nature remains neutral with regard to jurisdictional claims in published maps and institutional affiliations.